Amphibole Control on Copper Systematics in Arcs: Insights from the Analysis of Global Datasets

Nicholas D. Barber[1*], Marie Edmonds[1], Frances Jenner[2], Andreas Audétat[3], and Helen Williams[1]

[1]Department of Earth Sciences, University of Cambridge

[2]School of Environment, Earth, and Ecosystem Sciences, The Open University

[3]Bayerisches Geoinstitut, University of Bayreuth

April 28th, 2021

This manuscript was originally submitted for publication in Geochimica et Cosmochimica Acta on January 5th, 2021, and re-submitted following positive peer-review on April 28th, 2021. Please note that this manuscript is still under review. An earlier version of the manuscript was rejected with constructive comments from Nature Communications. Subsequent versions of this manuscript may have slightly different content than the original version. If accepted, the final version of this manuscript will be available via the 'Peer-reviewed Publication DOI' link on the right-hand side of this webpage. Please feel free to contact Nick (ndb38@cam.ac.uk) with any feedback. We welcome your comments!

Abstract

Copper, sourced from porphyry deposits formed in arc settings, is a critical resource, and is primarily sourced from magmas. However, the processes that shape the copper contents of arc magmas are up for debate. Existing models place emphasis on different petrological agents that explain large-scale trends in copper systematics. Previous studies have noted the 'Cu paradox,' where the magmas with high Sr/Y ratios, indicative of ore-forming potential, have the lowest copper concentrations. Here we compile a multidimensional database of volcanic whole rock compositions and couple it with simple petrological models to elucidate the controls on volcanic whole rock compositions with respect to Cu. We show that calc-alkaline, high Sr/Y magmas undergo major element modification caused by extensive amphibole and/or garnet fractionation, which promotes sulphide precipitation and copper depletion. We demonstrate the importance of amphibole fractionation as a globally important process that promotes both calc-alkaline differentiation and sulphide fractionation in arc magmas, as well as its role in signalling the right set of chemical conditions in magmas that ultimately feed copper porphyry deposits. This work also raises the possibility of amphibole as a geochemical and petrological indicator of potential porphyry-forming conditions in a magma, which we show should be readily detectable by a combination of different geochemical metrics. Despite their paucity in copper, high Sr/Y magmas are associated with porphyry deposits, implying that the propensity of magmas to form such deposits depends on factors other than a magma's bulk copper content.

1 Introduction

Copper (Cu) is economically important owing to its role in the development of electrical components and its critical status in the transition to green energy[1]. Porphyry deposits, which are temporally and spatially associated with arc magmatism (Figure 1), account for over 70% of global Cu ore production[2], and significant amounts of Au and Mo[2]. Great progress has been made in developing a general model of porphyry development[3–9], yet more work needs to be done to understand how these processes are expressed in modern volcanic environments[10]. Prevailing magmatic models of Cu porphyry formation focus on two important processes, which may promote Cu enrichment, transport, and deposition in and around porphyry stocks: (i) the saturation of the magma in sulphide (an Fe and S-bearing liquid or mineral phase), into which Cu partitions strongly[11–17], a process which may deplete the magma Cu when sulphide fractionates, but may also enrich a magma if sulphide is remobilised by hotter or more oxidised magma[6,18–20]; and (ii) the exsolution of a volatile phase, which may unmix to a brine and vapor at low pressure[10], into which Cu and other metals partition and eventually precipitate from, leading to ore deposition[5,21–23].

A number of models have been proposed to explain how these processes may enhance a magma's potential to eventually go on and form a mineralized deposit. It has recently been suggested that sulphide saturation may be avoided by simultaneous Fe depletion and auto-oxidation caused by garnet fractionation[7]. Garnet's preference for Fe^{2+} leaves residual magmas enriched in Fe^{3+}[7]. This in turn produces a more oxidized and evolved melt (with higher S^{6+}/S^{2-}), which pushes the magma further away from sulphide saturation and may even trigger the dissolution of existing sulphides. It was proposed that this garnet-mediated process could enrich the melt in Cu, which could then be transferred to fluids when porphyry formation commences[7]. Alternatively, others have argued

that sulphide accumulation may be critical to later ore development by pre-concentrating a reservoir of localized sulphides at the base of a magma reservoir[6], where it is remobilised by intruding hotter or more oxidised magmas, thereby enriching these magmas in Cu[6].

However, other studies have de-emphasized the importance of magmatic Cu contents as an indicator of ore potential[3,24], promoting instead the importance of magmatic water content[9,25,26], time scales of magma differentiation[27], and larger magma volumes[28] as some of the critical controls on the capacity of a magma to produce a porphyry. Nonetheless, nearly all models agree that the process of sulphide saturation is important for understanding eventual ore formation. Sulphide saturation is a complex process mediated by temperature, pressure, and silicate melt composition, and thanks to continued empirical work the factors leading to sulphide saturation in silicate melts are increasingly well understood[29–34]. However, it is presently unclear (i) what petrological processes in arc magmas will promote, delay, or are simply associated with sulphide fractionation, and (ii) whether the early fractionation of a sulphide, and associated loss of Cu, is detrimental to later porphyry formation[18].

One reason that these outstanding questions remain is the measure of sample bias in our existing understanding of Cu systematics. Crucially, we need to establish what generic petrological processes, if any, can explain the abundances of Cu in arc magmas in all major subduction zones. In order to address this need, we compiled a large global database of volcanic arc whole rock compositions (Figure 1). The ArcMetals database (N = 55,795) contains data from 17 arcs, encompassing geochemical and contextual information such as major, trace element and radiogenic isotope compositions, geology, location, and geologic age (see Methods), expanding on the approach taken by[3,7,20,26,35,36]. Combined, these parameters allow us to explore Cu systematics in all arc settings. We

interpret the generic features of ArcMetals with respect to Cu systematics using models of silicate melt differentiation[37] and sulphide saturation[29] based on recent high-quality experimental studies. This work pushes forward our understanding of key magmatic processes occurring in arcs that influence the capacity of magmas to develop ore deposits. Furthermore, this work provides a framework for further interrogation of major mineral controls on chalcophile metal behaviour in specific volcanic arcs.

2 Methods

2.1 ArcMetals: Data Sources and Compilation

2.1.1 Database Design

This paper presents a new compilation of existing arc volcanic whole rock chemistry called *ArcMetals*. This database was compiled with several crucial design distinctions in mind which distinguishes it from previous databases. First, we wanted the database to be fully integrated with the spatial dimension of the data. Hence, much of the compilation work takes place in a Geographic Information System (GIS) environment, where we can control and append geophysical and tectonic datasets. As discussed in greater detail both below and in the Supplement, this approach afford us several advantages over prior compilations. Here we take advantage of recent advances in the application of data science and Geographic Information Systems (GIS) in geochemistry, allowing us to build on prior studies that were based on simpler data compilation routines[3,7,20,25,35,36] in the initial compilation and filtration of GeoRoc data, combining existing petrological datasets in ore systematic ways. Subsequently, we apply a range of geospatial techniques to append the maximum amount of geophysical data to this compilation without compromising the extent or quality of this data. This

latter step is documented in detail in the Supplement, and is what sets this compilation apart from many previous datasets.

2.1.2 Geochemistry

Sample geochemical and analytical data were collected from the GeoRoc ([38]) database. These data were compiled using open source python code, available on GitHub (see link). Initially, 19 arc magma datasets were included in the database, but the Kermadec and Banda files contained so few data upon filtering, that they were ultimately omitted (Figure 1). Data for arc volcanic rocks were compiled (see Supplement). Before filtering, the fully compiled database contained $>$ 200,000 records. In order to maximize the number of measurements per sample, six filters were applied to the initial compilation: (1) records with data obtained before 1960 C.E. were removed; (2) records with no recorded analytical technique were removed; (3) only those records pertaining to measurements by X-ray fluorescence (XRF), secondary ion mass spectrometry (SIMS), electron microprobe (EPMA), thermal ionization mass spectrometry (TIMS), inductively-coupled plasma mass spectrometry (ICP MS), laser ablation inductively-coupled plasma mass spectrometry (LA ICP MS), and Fourier transform infra red (FTIR) spectroscopy were retained; (4) the database was reduced to individual records where sample name, material type (whole rock, glass, or inclusion), and analytical technique were the same (e.g. if 1 whole rock sample had 4 records in GeoRoc measured using XRF, this filter would reduce the 4 records to one average for XRF); (5) records with the same sample name and material type were averaged and collapsed into one record. This had the effect of combining a sample's ICPMS measured trace elements with its XRF derived major elements; (6) samples that had the same element measured more than once using the same technique were removed. This filter only affected a small subset (a few hundred) samples, but having it in place makes it easier to

quantify analytical errors (see Supplement). Before plotting, the final database was filtered to only include those magmas with a reported loss on ignition (LOI) less than 3.5 wt.%, following standards in the literature[25]

2.1.3 Geophysical Parameters

Several global geophysical datasets were appended to the main database using the geospatial software Quantum Geographic Information System, or QGIS 3.10. The data appended included subducting slab surfaces and geometry generated from extensive seismic records (slab dip, depth to slab, slab thickness)[39] , crustal thickness ([40]), and subducting plate sediment cover thickness ([41]). Every sample record in the database was linked to the geophysical datasets, which have good global coverage at a resolution of 10-100 km^2. A sub-population of database records had additional geophysical data appended based on their proximity to volcanoes analyzed in Syracuse et al. 2006[42]. These data included convergence rate, slab thermal parameter, and slab age[42]. The full QGIS methods and compilation scripts can be found in the Supplementary Information Section.

3 Results

We present summaries of global volcanic whole rock geochemical data in Figures 2-5 and 9. These are discussed and interpreted in section 4, in light of modeling done to validate these trends (Figure 6-8). Figure 2a shows volcanic whole rock Sr/Y versus SiO_2, colour-coded for the different arcs (Figure 2b), Cu content (Figure 2c) and crustal thickness (Figure 2d). It has been shown that magmas fertile for porphyry Cu deposit formation have high whole rock Sr/Y ratios at intermediate to felsic magma compositions (Figure 2,[25,35,43]). The Sr/Y ratio, which compares the Large Ion Lithophile Element (LILE) Sr to the high field strength element (HFSE) Y, is widely regarded as a proxy for high pres-

sure fractionation of hydrous arc magmas[20,25,43]. Strontium abundances during fractionation are primarily controlled by plagioclase[44], whereas Y abundances are controlled primarily by amphibole and garnet, as well as some minor phases like titanite[45]. The ratio of plagioclase to amphibole crystallized in a fractionating arc magma is decreased under conditions of high H_2O activity[46,47], which simultaneously stabilizes amphibole phases which incorporate H_2O into their structure[48]. Thus, a hydrous magma should see abundant amphibole fractionation early in its differentiation in the mid to deep crust (up to 50 km.,[49–51]) and late-stage plagioclase crystallization at or near volatile saturation in the upper crust[25]. This fractionation sequence will result in an elevated Sr/Y ratio in deeply derived andesitic to dacitic magmas with significant amphibole[25].

Figure 3 shows MgO versus total FeO plots for global volcanic arc whole rocks, colour-coded for Cu contents (Figure 3a and c), Sr/Y (Figure 3b) and crustal thickness (CT; Figure 3d). These plots show that whole rocks with high Cu contents lie along a tholeiitic trend (with Fe-enrichment), whereas those whole rocks that lie along the calc-alkaline trajectory (with Fe depletion) are copper-poor. These rocks also have the highest Sr/Y[25]. These observations are consistent with previous work[3,7,20,52,53].

We identify the principal processes responsible for the geochemical trends shown in Figures 2 and 3 using rare earth element (REE) concentrations (Figures 4 and 5). Figure 4 shows data sorted so that the highest [Cu] and Sr/Y points are placed "on top" of the data cloud to ensure the reader is not missing any of the highest [Cu] and Sr/Y points. However, there are many more low [Cu] and Sr/Y points, as shown in the Supplement via 3D scatter plots set up using the same axes and plot design (Figure S10). The schematics at the top of both Figures 4 and 5 show vectors for the fractionation of garnet, amphibole, olivine, plagioclase, orthopyroxene and clinopyroxene using an index of REE

plot curvature, Dy/Dy*[54]. Essentially, Dy/Dy* estimates the relative depletion of the middle rare earth (MREE) Dy in relation to its light (LREE) and heavy (HREE) counterparts. The Dy/Dy* metric makes a weighted determination of the slope and shape of an REE spider diagram with respect to Dy, as:

$$\frac{Dy}{Dy*} = \frac{Dy_N}{La_N^{4/13} + Yb_N^{9/13}} \tag{1}$$

Dy/Dy* is of particular use for tracking amphibole/cpx and garnet fractionation[7,54–56] in rock suites. Additionally, the trajectories for melting in the garnet source field are plotted following[54]. The ratio Dy/Dy* tends to be lowered by amphibole and clinopyroxene fractionation. These phases will deplete Dy relative to Yb. Olivine, plagioclase, and orthopyroxene will drive Dy/Dy* towards higher values, as these phases do not incorporate Dy into their structure and thus Dy will be enhanced relative to light (LREE) and heavy (HREE) rare earth elements. Garnet fractionation will move Dy/Yb to higher values during fractionation (i.e. deplete Yb relative to Dy) while simultaneously increasing Dy/Dy*. Mantle melting in the presence of garnet will lead to more moderate values of both Dy/Yb and Dy/Dy* if a garnet rich source is extensively melted (see Discussion section for more details).

The REE systematics of the global database can be further explored using a statistical approach[57], which compares parameters describing the shape of chrondrite-normalized multi-REE plots (Figure 5). The REE polynomials, symbolized by λ, describe the shape of REE curves[57] based on multivariate statistics across all REE elements.[57] The polynomials are determined from the following calculation in orthogonal form:

$$\ln([\mathrm{REE}]/[\mathrm{REE}]_{\mathrm{CI}}) = \lambda_0 + \lambda_1 \mathrm{f}_1^{\mathrm{orth}} + \lambda_2 \mathrm{f}_2^{\mathrm{orth}} + \ldots \tag{2}$$

Where the f variables represents polynomials of REE atomic radius (r_{REE}), chosen to avoid co-correlation of the λs[57]. A schematic at the side of Figure 5 shows the effect of fractionation of amphibole/cpx and garnet on REE systematics, expressed in terms of $\lambda 1$ and $\lambda 2$. Figure 5 is subsampled to only color magmas for Cu (Figure 5a) and Sr/Y (Figure 5b) where the whole rock composition shows Sr/Y $>$ 50 (considered the "high Sr/Y" field in Figure 3). In the section below we discuss these geochemical data, present an interpretative framework, and place it within the context of previous studies.

4 Discussion

4.1 Geochemical Characteristics of High Sr/Y Magmas

We follow the lead of Loucks (2014), in recognizing the close association between high Sr/Y magmas and porphyry mineralization (Figure 2a[25]). Following this approach, this work shows that high Sr/Y magmas show an association with continental arcs such as Mexico, the Andes and the Cascades (Figure 2b and Supplementary Material), a low mean whole rock Cu concentration ($<$ 50 ppm, (Figure 2c) and thicker crust (mean 40 km, Figure 2d) consistent with previous studies[3,20,35]. These same magmas also sit in the high Dy/Yb, low Dy/Dy* quadrant of Figure 4b, and the high $\lambda 2$, high $\lambda 1$ quadrant of Figure 5b. To confirm whether the mean Cu and crustal thickness differences in Figure 2 between high and low Sr/Y magmas is statistically robust, these values were compared using a two-way analysis of variance (ANOVA) hypothesis test, and subsequent Tukey's highly significant difference test. The null hypothesis tested in all cases was that the mean of a given measure is the same between two groups. The likelihood this is due to random chance is calculated using an F statistic, given by:

$$F = \frac{\Sigma n_j \left(\bar{X}_j - \bar{X}\right)^2 / (k-1)}{\sum \Sigma \left(X - \bar{X}_j\right)^2 / (N-k)} \tag{3}$$

Where n_j = the sample size in the jth group, $\bar{X}_j$ is the sample mean in the jth group, $\bar{X}$ is the overall mean, k is the number of independent groups in the analysis, and N is the total number of observations in the analysis[58]. This F-statistic is compared to a a critical-F at a given confidence threshold and degrees of freedom. After determining the p-value, which is a simple but easily misinterpreted measure of the likelihood of difference between the means occurring due to random chance, the difference between the different treatments (e.g. different arcs, different Sr/Y groups) is compared using a Tukey HSD test, which calculates the following test statistic:

$$q_s = \frac{Y_A - Y_B}{SE} \tag{4}$$

where Y_A is the larger of the two means, Y_B the smaller, and SE the standard error of the sum of the means. See the Supplement for detailed plots comparing the test statistics, tables with statistical outputs and constraints, and the code used in these analyses. The mean (1) Cu and (2) crustal thickness of the high and low Sr/Y groups in Figures 2c and 2d have been compared, respectively, using ANOVA tests, and these differences have been shown to be statistically significant (p « 0.005) (see Supplementary Information for statistical tables).

The low mean Cu concentrations ([Cu]) in whole rocks associated with higher Sr/Y (Figure 2c) highlights the so-called 'Cu-paradox'[7], where Cu is present in low abundance in the magmas that appear to be most capable of forming ore deposits. Observations such as these have been used to support porphyry formation models where crystallization of sulphide removes Cu from the silicate melts, to be later remobilized by one of several petrological processes[6,7,18,19].

However, it is also possible that melt [Cu] depletion may have little bearing on whether a magma goes on to form an ore deposit[3,24]. While this initial analysis confirms the findings of prior studies that magmatic [Cu] is significantly lower in high Sr/Y magmas on a global scale[3,7,20], the petrological processes driving this association have not yet been resolved. To address this, empiricla datasets are combined with simple trace element partitioning and sulphide saturation models are applied to better understand what petrological processes are associated with high Sr/Y and low Cu in magmas.

4.2 Amphibole vs. Garnet Signatures

Globally, it can be seen that both low Cu (Figure 3a) and high Sr/Y (Figure 3b) volcanic whole rocks follow a calc-alkaline path, showing consistent Fe loss with decreasing [MgO] (paralleling the high Sr/Y ellipse in Figure 3d). Similar results were obtained by earlier data compilations[7,20,26,35]. Figure 3c and 3d plot the binned FeO and MgO concentrations that have been smoothed to show average FeO, MgO, Cu (Figure 3c), and crustal thickness (Figure 3d) at 0.05 wt.% MgO intervals. Figure 3c also shows the fractional crystallization paths of experimentally synthesized and oxidized andesites and basalts[37], which also lie on the calc-alkaline trend displayed by high Sr/Y magmas (more detail on these in section 4.3).

Analysis of the global database suggests that high Sr/Y arc magmas share key petrological features: they may undergo extensive fractionation of amphibole +/- clinopyroxene and garnet (they extend into the bottom left quadrant for Figure 4, upper right in Figure 5) and develop low Cu abundances during progressive differentiation (Figure 4a, 5a). Whole rock compositions with the highest Sr/Y ratios are characterized by concave-up REE profiles, where there is both HREE depletion and overall enrichment in the LREE (Figure 4b). Figure

4b shows a strong preference for high Sr/Y magmas to sit in the bottom right "garnet-influenced" quadrant (High Dy/Yb, low Dy/Dy*), and Figure 5a and 5b show many high Sr/Y whole rocks sitting near the amphibole fractionation and garnet source field in $\lambda 1$ vs. $\lambda 2$ space (higher $\lambda 1$, higher $\lambda 2$). While there is a clear association between high Sr/Y, low Cu magmas and the amphibole fractionation field, the location of high Sr/Y magmas at low Dy/Dy* and moderate Dy/Yb can also be explained through a magma formed in the "melting of mantle garnet" field (bottom right quadrant) which subsequently experienced (1) garnet fractionation at pressures around 1.2 GPa[51], followed by (2) amphibole +/- clinopyroxene fractionation at lower pressures[51]. Whatever the exact sequence of processes, a magma plotting in the bottom-right quadrant of Figure 4 must have experienced some HREE depletion and/or LREE enrichment to match the predicted patterns of this metric[54]. Additionally, all magmas have a starting REE profile that may not begin at the "crosshair" intersection of the two bold black lines (defined for chrondritic-derived melt[54]). Rather, each magma is likely derived from a mantle source with a unique REE profile defined by prior melt extraction, metasomatism, and other pre- and syn-melting features. Correcting for such source features is beyond the scope of this work, but would be an interesting area of the global database to explore more fully. The complexities of the petrogenesis leading to changes in Dy/Dy* should make us cautious about using the Dy/Dy* systematics alone to diagnose the petrogenesis of high Sr/Y magmas. Rather, any petrogenetic process proposed here must be validated by other independent metrics, empirical observations, and/or modeling.

This garnet to amphibole/cpx sequence may only be piecemeal at shallower pressures, where amphibole/cpx will dominate as a fractionating phase outside the stability field for garnet[51]. Thus, while the importance of amphibole

in these systems will be demonstrated further, garnet likely also plays an important role, especially in the deep roots of arc magmatic systems[7,51,59]. By the same logic, the influence of clinopyroxene cannot be ruled out, as cpx will produce a similar compound fractionation trend as suggested by the blue line for amphibole-garnet in Figure 4a, albeit with a steeper slope. Clinopyroxene is one of the most common minerals in arc volcanic rocks, and empirical determinations of pyroxene stability indicate that amphibole-friendly magmatic conditions are comparably favourable for clinopyroxene[37,51]. However, amphibole is favoured over clinopyroxene at higher magmatic water contents[51] and lower temperatures[37,51] i.e. conditions more common in andesites stored in the shallow to mid-crust (aligning with the conditions of magmatic storage prior to porphyry formation[4]). Furthermore, the λ plots show less ambiguously that high Sr/Y, low Cu magmas often have a much steeper slope, consistent with amphibole control as opposed to cpx (Figure 5a, 5b). This emphasizes the importance of combining geochemical metrics to get the most out of whole rock data.

Garnet fractionation has gained popularity in the recent literature as a potential ore fertility mechanism[7,55,59]. Experiments have shown that garnet is stabilized as a fractionating phase at pressures above 0.8 GPa (approximately 24 km. depth)[51,60] and where melt water contents are high (above 4 wt. %)[51]. Direct evidence of garnet in arc magmas is rarely found in modern volcanics, but it has been found commonly in fossil arc systems[61]. Whether ancient or modern, where garnet can be seen widely in arc systems is in the lower crust cumulate lithologies of exhumed "arc roots," sections like the type section in Kohistan, Pakistan[62–64]. Models developed for the mantle wedge underlying Central America found evidence for the presence of mantle heterogeneities rich in garnet-peridotite or garnet pyroxenite lithologies[65]. Melting of such mantle

garnet "veins" would impart a signature with higher Dy/Yb than the arc array, as discussed in detail in previous work[54,65].

While the role and importance of garnet fractionation is not disputed in explaining the occurrence of some magmas with low [Cu] in thicker-crust arcs[7,59], this analysis suggests that amphibole is also an important candidate for moderating global arc Cu systematics as shown in Figures 4 and 5. The importance of amphibole has been previously proposed in the context of porphyry deposits[25] and the broader controls on magmatic Fe^3, although in both of those cases REEs were not used as a metric to measure amphibole's presence. Amphibole fractionates in many arc magmatic environments at moderate (15-40 km.) depths[49,51], while also being verifiable petrographically in volcanic products, either as a primary phase or as an exhumed xenolith[66]. Like garnet, amphibole is much more stable at high melt H_2O contents[37,51,60], but unlike garnet it predominates at moderate, not only deep crustal depths (20-55 km[49–51]) rather than just deep depths. For many of the reasons the garnet hypothesis is favored, amphibole can be similarly supported as an important chemical control on the bulk chemistry of arc magmas. Amphibole will be stabilised at moderate to temperatures (between 800 and 1050 °C[37,51]), moderate to high pressure (0.7 - 1 GPa[49,51]), and high water contents[51]. These results show, consistent with the literature, the strong and unambiguous importance of the association between amphibole in the fractionating assemblage and high Sr/Y magmas[3,9,20,25]. However, the mechanism by which amphibole obtains such an association, particularly with regards to [Cu], has not been explored in great detail in previous studies.

4.3 Amphibole Control on Melt Chemistry and Sulphide Stability

To understand how amphibole is able to affect these global Cu trends, it is necessary to show how amphibole can provide a link between high Sr/Y, calc-alkaline, potentially porphyry-developing magmas, and their low Cu contents. This is first done by analyzing the empirical results of a well-constrained series of isobaric fractional crystallization experiments[37] in the context of the low Cu, high Sr/Y magmas centered in this work (section 4.3.1). These empirical datasets are integrated with a trace element partitioning (reconstructing Cu, Ni, Sr, Y, and REE systematic) (4.3.1) and sulphide saturation (4.3.2) model to estimate the impact of amphibole on melt chemistry and subsequent sulphide systematics. Special attention is paid to amphibole's method of changing melt chemistry, with regards to the calc-alkaline differentiation trend discussed in Figure 3. All of these empirical and modeled observations are synthesized together by a simple mass balance model to link the fractionation of amphibole in andesites with the stabilization of sulphide and subsequent depletion of [Cu].

4.3.1 Analysis of Empirical Datasets

Trace element abundances of experimental results from an existing empirical study[37] were modeled to constrain the effect of amphibole on the liquid line of descent in arc magmas, in order to understand how amphibole fractionation may connect major and trace element systematics under high Sr/Y-favoring conditions. The experimental study in question ran isobaric experiments under equilibrium (EC) and fractional crystallization (FC) conditions at 1.0 GPa and from 1200 to 720 °C on hydrous oxidized basaltic[67] (called "FC Mb AuPd" in the original work) and oxidized andesitic (called "FC ba AuPd" in the original work) melts[68] .

The experimental data used in this works' model[37] were prepared by transcribing Table 1 (starting conditions), Table 2 (modal abundances of minerals at each experimental temperature step), and Table 3 (glass and amphibole compositions, determined by EPMA) into Supplemental Data Table 4 of this work. In Ulmer et al. 2018, major elements were the only measured chemical species. Starting abundances of Ni, Cu, Sr, Y, and all REEs were taken from the trace element compositions of the relevant starting materials[46,67,68], and used to model the partitioning of trace elements into fractionating mineral phases following the methods of Shaw 2006[69]:

$$\frac{c_l^t}{c_o} = F^{D-1} \tag{5}$$

where t = timestep *t* in a given experiment, corresponding to a specific set of T, P, and X_i conditions. Also called *run number* in 'ud' database; c_l^t = concentration of an element in the residual liquid; c_o = initial concentration of an element in bulk liquid, before fractionation; F^t = fraction of residual liquid $\frac{L}{L_o}$; D^t = "Bulk D," or weighted sum of whole rock partition coefficients:

$$D^t = \sum_{i=0}^{\infty} X_i^t * D_{i-l}^t \tag{6}$$

where X_i = mass fraction of mineral *i* in accumulated solid fraction, and D^{i-l} = partition coefficient (or K_d) between mineral *i* and liquid *l*. Final form of Eqn. 5 requires that c_l is solved at each experimental step in the differentiation sequences:

$$c_l = c_o * F^{D-1} \tag{7}$$

The effect of these trace element models on elements like Cu and Ni can be found in the Supplement (Figure S11). Note that of the three FC experiments

total in the experimental database, only two are focused on in this work (the oxidized runs). The results from Ulmer et al. 2018 experienced some empirical complications around 900 °C, and the remaining melt fraction (F) and resultant melt chemistry was reversed from what one would expect to occur naturally (decreasing F with decreasing T). In order to make modeling these results as straightforward as possible, runs 10-12 and 9-11 were discarded from the oxidized andesite and oxidized basalt experimental runs respectively. One of the most remarkable features of these empirical results is the well constrained liquid line of descent (LLD) for calc-alkaline, hydrous, moderately oxidized magmas, and the resulting association between LLD and major mineral phases like amphibole. Also remarkable is this empirical datasets constraint of the changes of fO_2 with magmatic differentiation[37].

4.3.2 Comments on Amphibole's Effect on Mg#

Experimental work[37,49,51,70] has already implicated amphibole as one of the most important phases controlling major element characteristics in high pressure calc-alkaline magmas. However, invoking amphibole as an important agent of melt chemistry change, as suggested f rom Figures 4 and 5, raises the question of how amphibole, with an Fe/Mg exchange coefficient ratio of around $\tilde{0}.3$[70], can maintain the consistent melt Mg# trend observed in calc-alkaline suites (see Figure 3, high Sr/Y trend). The calc-alkaline trend observed in high Sr/Y magmas sees a constant decrease of FeO with MgO, meaning that equal proportions of both elements have to be leaving the melt to explain the changes in melt chemistry. Despite the higher exchange coefficient of Mg in amphibole as compared to Fe[49], some empirical work has noted that the majority of major element differentiation in metaluminous/peraluminous magmas should be controlled by amphibole at the relevant pressure and temperature conditions[51].

To test this, the relationship between amphibole, melt Mg#, and FeO con-

tents from the oxidized FC experiments[37] has been plotted in Figure 6. Where amphibole stabilizes at 1050°C (Figure 6a), the Mg# of the melt does not see the predicated rapid Mg# drop off as a function of either temperature (Figure 6a) or melt FeO wt.% (Figure 6b and c). Instead, melt Mg# decreases smoothly through the amphibole stability field. Two major factors help to explain this trend: (1) coexisting phases crystallizing at the same time as amphibole, and (2) amphibole's increasing FeO content and correspondingly lower Mg# as the magmas cools. Starting with the former, phases including clinopyroxene, garnet, plagioclase, ilmenite, and magnetite (in order of appearance) contribute to changes in melt chemistry in the andesite, and in the basalt, this series of other minerals also includes spinel. By mineral chemistry, phases like ilmenite, magnetite, spinel, garnet (Fe/Mg exchange coefficient of around 0.7[51]), and even clinopyroxene contain enough iron to explain the consistent decrease in FeO seen in the empirical data modeled here. It should be noted however that amphibole is one of the dominant minerals in the fractionating sequence following its initial stabilization at 1050°C - thus, a good portion of the changes in melt chemistry must be attributed to amphibole. Amphiboles stability may in fact be a marker all on its own of the right conditions contributing to calc-alkaline differentiation; contrast the trends seen in Figure 3 for the oxidized andesite and oxidized basalt (Figure 3c) with that of the reduced basalt (FC ba Pt-C), where the lack of amphibole contributes to the more tholeittic pattern of differentiation and a lack of FeO depletion.

Furthermore as the empirical[37] melts' reach temperatures below 900°C, Figure 6b and 6c show that amphibole itself begins to take on more iron into its structure. The stable amphibole species steps down from paragasite at temperatures $>$ 900°C, to tschermakite (900°C), tschmerkatic hornblende (800 °C), and finally magnesio-hornblende (720°C) at the end of each fractional crystal-

lization experiment (amphibole names follow established nomenclature[71]). Not only does the FeO w.t% of amphibole increase with greater degrees of differentiation, but Figure 6c sees a decrease in the Mg# of fractionating amphibole's as well. Figure 6 shows that, consistent with the literature[37,49,51,70], amphibole is not only associated with fractionating assemblages moving an arc magma towards calc-alkaline differentiation, but it can indeed alter the FeO content of a melt, in spite of its general preference for Mg cations over Fe. This extended discussion of amphibole's impact on Fe is pertinent to the crucial element of modeling done in this study, namely Fe's impact on sulphide saturation.

4.3.3 Integrating Sulphide Models into Empirical Results

To see whether major and trace element changes in a silicate melt affect the stability of sulphides in the melt requires an empirical model of sulphide saturation. Sulphide saturation is described by the experimental parameter, "sulphur content at sulphide saturation," or SCSS[72]. Generally, SCSS is negatively correlated with pressure[72] and positively correlated with temperature[30,34,72], melt H_2O content[73], melt FeO, Cu and Ni contents[12,30,72 12,29,30], and oxygen fugacity (fO_2)[31,34,74]. For mid-ocean ridge basalts, melt FeO content, oxygen fugacity (fO_2), temperature, and pressure are the main drivers of sulphide saturation[12]. In arc magmas, higher water and sulfur contents[21,75] coupled with higher oxidation state[3,31] cause the SCSS to respond differently as compared to MORB, though major elements like FeO still play a major role. For most arc magmas, volatile and oxidation conditions lie outside the range for which many SCSS models are calibrated[72], with some exceptions[31,73]. Since most arc magmas have a considerable fraction of sulphur present as S^{6+}, they may instead saturate in anhydrite, which is much more soluble in silicate melts[33].

SCSS was modeled for the oxidized basalt and oxidized andesite runs (Figure 3, 5, 6-8), using the major elements[37] and modeled trace elements (Cu, Ni) of

the individual products as inputs using a new SCSS paramterization[29]:

$$\ln\left[\mathrm{S}^{2-}\right]_{\mathrm{SCSS}} = \Delta G^{O}_{FeO-FeS}/\mathrm{RT} + \ln C_{S^{2-}} - \ln a^{silmelt}_{FeO} + \ln a^{Sulf}_{FeS} \tag{8}$$

This SCSS method builds on the work of[30], and is very sensitive to the bulk silicate melt composition, the sulphide composition, Fe-Ni-Cu partitioning into that sulphide, and P and T at ranges appropriate for these models[29]. For all experiments, SCSS decreases with FeO and decreasing temperature (Figure 7a and 7b respectively)[72]. The SCSS values are initially calculated assuming the redox state of the magma will favor mainly S^{2-}[29]. To account for the likely abundance of S^{6+} , SCSS was calculated for a range of S^{6+} speciation end members based on the ΔNNO buffer values for $f\mathrm{O}_2$ measured in the modeled experiments. These values, 0.5, 1.0, and 1.5 ΔNNO, correspond to ΔQFM values of 0.78, 1.28, and 1.78 respectively (ΔNNO to ΔQFM conversion accomplished using the Excel tool "Calc-fO2-buffer' from http://www.kaylaiacovino.com/tools-for-petrologists/, using data from previous work[76]). These $f\mathrm{O}_2$ values translate to $\frac{S^{6+}}{S_T}$ values of 0.2, 0.75, and 0.95 following a simple correction scheme developed for oxidized magmas[77]:

$$SCSS_{Tot} = \frac{SCSS^{2-}}{\left(1 - \frac{S^{6+}}{\Sigma S}\right)} \tag{9}$$

This in turn is based on an earlier parameterization of S^{6+} as a function of ΔQFM buffer[31]:

$$\frac{S^{6+}}{S_T} = \frac{1}{1 + 10^{(2.1-2\Delta FMQ)}} \tag{10}$$

Figure 7 shows the results of modeling the different S^{6+} abundances in the

magmas by using different symbols denoting the different oxidation state of S in each empirical dataset. The onset of amphibole crystallization is shown both as function of FeO (Figure 7a) and temperature (Figure 7b). To aid the reader in understanding what major minerals are fractionating during the experiments, a schematic blue line has been added to Figure 7a showing the major controls on SCSS changes at different stages in the model. Where amphibole was the dominant fractionating phase in these experiments, there was only secondary involvement of minerals like garnet, magnetite, ilmentie, clinpyroxene, plagioclase, and spinel, though amphibole become less abundant as temperature continued to decrease[37]. High-temperature (>1050 °C) FeO loss is attributed to clinopyroxene and to a lesser extent orthopyroxene and olivine (only in the basalt), followed by a much more amphibole (as well as garnet) mediated lowering of SCSS at temperatures below 1050°C. These two FeO loss trends, clinopyroxene vs. amphibole mediated, are separated by a small but abrupt decrease in SCSS, which is a function of temperature change as clinopyroxene abundance decreases and amphibole starts to appear (the "drop-off" on the blue curve in Figure 7a).

The onset of amphibole fractionation is associated with a continued lowering of the SCSS, but no clear dramatic decrease (Figure 7a, b). However, if we consider conditions relevant to porphyry development, clinopyroxene in these experiments only fractionates at temperatures greater than 1050 °C, which should be less common in the sort of mid-crust, high water, low Cu and high Sr/Y magmas presumed to be important for developing porphyry systems. The comtinued drop in SCSS as a function of FeO (Figure 7a) can be attributed to other phases stabilzing alongside amphibole, and the increasing FeO and decreasing Mg# trends seen in amphiboles from Figure 6b and 6c. Since arc magmas usually contain bulk sulphur contents between 1000 and 2000 ppm (red box in Figures 7a and 7b)[75], these models confirm that most hydrous arc magmas are

at or near sulphide saturation[3,24] during most of their differentiation, and as a result will become depleted in Cu as sulphides are removed; this hypothesis can be verified by further modeling (see 4.3.4). Furthermore, these magmas demonstrate that even with $\frac{S^{6+}}{S_T}$ values approaching 0.75 at ΔQFM values greater than 1.2 (diamond and circle curves for andesite and basalt, respectively), sulphide fractionation can be pervasive.

The noticeable but not necessarily dramatic decrease in SCSS at amphibole-in is mediated by several competing factors: (1) As should be obvious from the SCSS paramaterization above, FeO is the crucial oxide driving much of the change in melt SCSS[29]. Of particular importance is the activity of FeO in the melt, a_{FeO}, which is affected by the activity coefficient of FeO γ_{FeO} according to Eqn. 8 (Eqn. 46 in original source[29]). (2) Different cations have a competing effect in this γ term. For example, MgO has a strong negative correlation with γ_{FeO}. This means that higher MgO will lower the activity coefficient of FeO, mitigating the drop in SCSS as would be expected from FeO loss alone. Should olivine or another mafic phase precede amphibole fractionation as is the case for the oxidized basalt, the comparatively lower MgO will lead to a strong increase in γ_{FeO}, magnifying the SCSS decrease. (3) By the same logic, the strong positive correlation between Na, K, and γ_{FeO}, implies that a loss of alkali elements will enhance SCSS reduction during amphibole fractionation. So the SCSS-buffering effect is mitigated in part by a strong decrease in the alkali content of the model melt, promoting the continued SCSS decrease seen in Figure 7. (4) The $\ln a_{FeS}^{Sulf}$ term, or the activity of the sulphide itself, has a large impact on SCSS. Related work has shown that the interplay between the Fe, Cu, and Ni abundances in sulphide is a strong control on the SCSS[30]. Hence, the models of Cu and Ni abundance in the trace element partitioning models included a small weight fraction (0.001) of sulphide fractionating at each

step, assuming the sulphide in question is a sulphide melt (see next section for details), and using partition coefficients for Cu and Ni between sulphide melt and silicate melt from[78]. These Kd's are 1070 for Cu, and 490 for Ni, taken from experimental run LY04[78]. The consistent decrease of Cu and Ni in the silicate melt leads to a concurrent decrease in the sulphide Fe/(Fe+Cu+Ni) content in the hypothetical sulphide, and a corresponding decrease in the SCSS. Finally, (5) the continual decrease in temperature at constant pressure as performed in these experiments strongly affects the SCSS in the preferred SCSS model[29]. This approach to modeling SCSS alongside calc-alkaline differentiated magmas shows the potential for amphibole to contribute to the modification of wholesale melt chemistry.

4.3.4 Mass Balance of Amphibole's Effect on S

Figure 7 shows the almost wholly linear decrease of modeled SCSS as the oxidized andesite and basalt runs progress. However, SCSS alone only tells half the story - to explain how amphibole fits into the story of the low Cu, high Sr/Y magmas concerned in this work, there needs to be a compelling link between this decrease in SCSS and the melt's sulphur content [S]. One way to demonstrate this is to take a similarly simple FC modeling approach as was done for the trace elements during the crystallization of the oxidized andesite and basalt. This is made possible if (1) there is a [S] imposed on each empirical melt, (2) the SCSS can be related to the [S] in such a way as to estimate the mass of sulphide fractionating at each step, and (3) the melt [S] can subsequently have been shown to have been perturbed by the modeled decrease in SCSS as a function of amphibole.

The results of these models are shown in Figure 8. Figure 8a shows the wt% of amphibole crystallizing in each experimental step[37]. Amphibole stabilizes at 35% crystallization (or F = 0.65) in the oxidized andesite (FC ba AuPd), and

63.70 % crystallization (F = 0.363) for the oxidized basalt (FC Mb AuPd)[37]. S contents in the melt were estimated based on inventories of [S] in the literature[75], as the starting experimental materials did not have reported measurements of volatile trace elements like sulphur[37,67,68]. The modeling done here assumed an oxidized arc basalt to have a starting [S] of 2000 ppm, or 0.2 wt.%[75]. Andesites should have already experienced some [S] loss, either as a consequence of degassing or as Figure 7c shows as a result of basaltic differentiation and subsequent sulphide fractionation - thus, the oxidized andesite series was modeled as having a starting melt [S] of 1000 ppm (corresponding roughly to the point the empirical basalt reached andesite-like melt compositions). Next, a simple mass balance was adapted from earlier work[32] on sulphide's effect on [Cu] in MORB composition magmas:

$$X_{sulf} = \frac{S_o - (SCSS)(X_{melt})}{S_{sulf}} \tag{11}$$

where X_{sulf} = the mass fraction of sulphide produced at each experimental step; S_o = the starting [S] in each step (initially 2000 and 1000 ppm respectively for the basalt and andesite); $SCSS$ = the modeled SCSS value[29]; X_{melt} = the remaining fraction of melt, or F and; S_{sulf} = the wt.% concentration of sulphur in the fractionating sulphide phase.

The goal of using this equation is to estimate the abundance of sulphide leaving the system once SCSS and [S] become equivalent, and by extension to model the decrease in [S] as a product of calc-alkaline differentiation. While the prior modeling in this work coupled with the original empirical results provide most of these parameters, this equation requires a fit to a particular sulphide composition, S_{sulf}. A suitable arc magma sulphide is required, one which was in equilibrium with basaltic to andesitic composition magmas, and which can also house significant amounts of Cu and Ni. The sulphide chosen was an

average sulphide melt modeled to be the parent of lower-temperature sulphides at Merapi volcano, Java, Indonesia[22]. Sulphide melts were preferred here over other sulphide phases like pyrrhotite or cubanite because they are often primary to the original melt, and only decompose into other, crystalline sulphide phases at lower temperatures[22]. The average sulphide melt from Merapi was estimated as having 38.2 wt.% S, 52000 ppm Cu, and $\tilde{2}$300 ppm Ni[22]. Fitting this value to Eqn. 11 allows us to construct a mass balance of sulphur in the empirical silicate melts analyzed in this study. The model results are presented as an Excel worksheet and corresponding Python code in the Supplement. As previously discussed, the silicate melts used here[37] correspond well to magmas stored at moderate depth under high H_2O, moderate to high pressure conditions. Thus, these results should be generalizable to many other hydrous arc andesites and basalts analyzed from ArcMetals and other compilations.

Figure 8b and 8c shows that amphibole crystallization corresponds to almost all of the sulphide fractionation and subsequent [S] loss in andesites. Starting from a basalt, amphibole stabilizes too late, such that amphibole plays only a marginal role in adjusting melt chemistry and corresponding sulphur and sulphide changes. Thus, conditions that favor olivine and pyroxene stability are conducive to widespread sulphide fractionation in the most primitive arc basalts, supporting our contention that most arc magmas experience pervasive sulphide saturation. However, this work has been much more concerned with the kind of andesitic, high Sr/Y magmas that would predominate in the mid- to lower crust in porphyry-friendly settings. In andesites, amphibole is the only major phase crystallizing when sulphides stabilize (Figure 8c). These coinciding trends are the combination of a lower S_o (due to earlier basaltic sulphide fractionation) combined with the earlier stabilization of amphibole and subsequent amphibole-mediation of melt chemistry changes. Thus it seems where an andesite begins

to fractionate, amphibole is the dominant mediator of sulphide fractionation. This fits with general observations that those high Sr/Y, low Cu magmas (with measurable Dy/Dy* and λ deviations consistent with amphibole) are likely intermediate composition trapped at depth. These results also suggest that it is amphibole-mediated changes in andesite melt chemistry, in turn a function of melt temperature, that lowers SCSS enough to cause sulphide precipitation as the [S] in the melt increases slowly as a an incompatible element until reaching the SCSS (Figure 8c). This again highlights the importance of amphibole as both a mediator of melt chemistry changes during calc-alkaline differentiation, and a signal of the optimal conditions for calc-alkaline and low Cu conditions in a melt. However, as Figure 7 showed, amphibole isn't radically changing melt chemistry all on its own. Rather, the conditions associated with amphibole crystallization (P, T, HO, fO2, melt chemistry) are conducive to a noticeable if modest decreases in SCSS, FeO (and other major elements), [S] and thus mass of sulphide fractionated and concurrent decrease in melt [Cu], where some but not all of these changes are directly the effect of amphibole. Equally important but not considered in depth in this work is the role of S degassing; should a magma degas significant volumes of sulphur, such that [S] in the melt falls well below the 1000+ ppm threshold set in Figure 8, there is little chance sulphides will stabilize, and every chance that remaining sulphides will resorb and breakdown.

The presence of sulphides in magmas has been reported by an increasing number of studies, in areas as diverse as Western North America[55], Kīlauea[77], Réunion island[79], Tolbachik volcano, Kamchatka[80–82], Merapi[22,83] and Ijen[84,85] volcanoes, Indonesia, the Ecuadorian[86] and Chilean Andean[56,59] volcanic zones, and even sulphide-rich hornblende cumulate xenoliths[24,87]. The models and analyses presented here (Figures 6-8), alongside the earlier compilations of whole rock major and trace element data (Figure 2 through 5), provide compelling

evidence that amphibole fractionation is a both a contributor to and signal of the cal-alkaline differentiation, extensive sulphide fractionation, and subsequent melt [Cu] depletion. Another Fe-rich mineral, magnetite, has been implicated in taking up substantial quantities of Fe^{3+}, which has been shown to lead to reduction of S from S^{6+} to S^{2-}. Since sulphide saturates at much lower [S] as compared to sulphate[19], higher proportions of S^{2-} will promote sulphide fractionation and metal loss. The crucial difference here is that amphibole's ability to promote sulphide fractionation and Cu loss is due to its reduction of total melt FeO and other oxides (like Na_2O and K_2O), and amphibole's broader stability throughout the differentiation history of an andesite. Furthermore, if enough amphibole (and co-stable phases like ilmenite) reduce FeO enough, it is possible that magnetite fractionation could be more limited.

4.4 Prevalence of Crystalline Sulphide Fractionation in Arc Volcanic Rocks

Our analysis of the global database demonstrates that amphibole fractionation, accepted as one of the drivers of high whole rock Sr/Y signals[9,25,35], can promote sulphide fractionation via Fe-loss and consequent Cu depletion in a typical calc-alkaline magma. The sulphide concerned is likely to at first be a sulphide melt[22], followed by a crystalline sulphide (e.g. monosulphide solid solution; MSS), which should predominate in the lower temperature conditions of an arc magmas as compared to MORB[17,87–89]. While the modeling in this study has been concerned with the primary sulphide melt, a further consideration that needs to be explored is whether there is direct evidence linking MSS fractionation with Cu depletion in arc magmatic sequences. Such a connection would not only emphasize the pervasiveness of sulphide fractionation in arc magmas, but would also further implicate minerals like amphibole, clinopyroxene, and garnet

as controls sulphide stability. This study attempts to provide such evidence by analyzing those whole rock compositions in ArcMetals that can be shown to have fractionated MSS sulphide. Figure 9 plots whole rock Cu/Ag vs. MgO , coloured for both Gd/Yb (Figure 9a), Dy/Dy* (Figure 9b), and for crustal thickness (CT) (Figure 9c). The motivation behind constructing such plots stems from the fact that Cu fractionates more strongly into MSS than Ag[13,78] (whereas the opposite is true in sulphide melts; sulphide melt fractionation should promote higher Cu/Ag), and such a ratio gives us the benefit of sensitively detecting the presence of a fractionating MSS at sulphide saturation[53]. A low Cu/Ag ratio, below average mid-ocean ridge basalt (MORB)[53,90] and continental crust[91], is consistent with crystalline sulphide fractionation and consequent Cu removal from the silicate melt[53] at lower temperatures than were modeled in Figure 8.

Gd/Yb (Figure 9a) is a proxy for garnet involvement in petrogenesis because Gd partitions less strongly into garnet than Yb[90], and has been used to infer the prevalence of garnet fractionation in the Andes[59]. The highest Gd/Yb ratios are associated with whole rocks with the lowest Cu/Ag for a given MgO content (Figure 8a), suggesting a direct correlation between the proportion of garnet fractionation and the proportion of crystalline sulfide fractionation. Owing to the complexities in analysing whole rocks for Ag, Cu/Ag datasets are rare and are currently biased towards the Andes data, though there are some measurements in other transitional arcs (Figure 8 symbols). There is no clear link between Cu/Ag in the whole rock and crustal thickness plot, but the very thickest crust (>40 km) is associated with evolved volcanic rocks, with a higher Gd/Yb (indicating garnet involvement) and low Cu/Ag. Figure 8b shows that lower Dy/Dy*, indicative of amphibole, is also associated with low Cu/Ag, evolved magmas. Thus, both garnet and amphibole are implicated in the petrogenesis of magmas that have experienced the most sulphide fractionation. One drawback

to using Cu/Ag as a proxy for sulphides in the global database is the dearth of available Ag and other chalcophile data in the literature. Only in the past 5-10 years have Ag and other difficult to measure elements become easily measurable using ICPMS[53,56,59,77,92]. As studies reporting suites of chalcophile elements in magmatic systems grow, future iterations of this database may yet be able to make broader, more detailed analysis of Cu/Ag in arc systems. Furthermore, our earlier modeling (Figure 7 and 8) suggest that a proxy like Cu/Ag is not necessary to confirm sulphide fractionation, as sulphide fractionation should be a ubiquitous phenomenon in arc magmas, thanks to changes in SCSS mediated by phases like amphibole. However, natural data, without the benefit of the kind of thermodynamic knowledge available in empirical datasets, can still benefit form chalcophile trace element ratios like Cu/Ag

It is worth noting that the Gd/Yb content of a magma could be affected by both garnet fractionation, or melt-derivation from a garnet rich source rock. If the latter, one would expect small fractional melts to have high Gd/Yb followed by progressively lower Gd/Yb as more and more Gd poor minerals melted out. To pick apart these competing REE trends (shown schematically in Dy/Dy* space in Figure 4, and in λ space in Figure 5) is beyond the scope of this work. Prior work on Cu/Ag establishes that particular volcanoes in the Andes likely experienced garnet fractionation as opposed to a mantle garnet signature[59]. One way to assess how widespread mantle-garnet melting is as reflected in whole-rock geochemical records would be to compare a suite of garnet-fractionating rocks to a suite of candidate garnet-melting rocks, like those analyzed for REEs in Central America[65]. A few well constrained cogenetic suites of rocks, analyzed for REEs and plotted as a liquid line of descent in Dy/Dy* and λ space would show what the relevant differences, if any, there are between garnet fractionation and garnet melting in complex natural magmas.

Our schematic model (Figure 10) emphasizes the primary importance of amphibole fractionation and the related importance of garnet/clinopyroxene fractionation[7]. This work emphasizes the importance of amphibole as a potentially widespread petrological-control mechanism that explains many of the generic features of high Sr/Y magmas. The global applicability of this amphibole-centred model complements garnet fractionation models, which work best in arcs with mature magmatic columns, deep brittle-ductile transitions (which promote longer residence times of magma in crust[7]), and thicker crusts[7,59]. This amphibole model also complements the more immature arc focused magnetite fractionation models, which work best in young island arcs and/or back-arc basins[19,90]. Our amphibole-centered model should be viewed on a continuum with these other petrological models, where water-rich, calc-alkaline trending arc magmas stored in the mid to deep crust (15-50 km.) will fractionate amphibole and stabilize sulphide in "semi-mature" arcs (called "immature continental arcs" as proposed in Lee et al. 2020, Figure 8b[7]). The exact depth of storage, temeprature, fO_2, and amphibole stability in these magmas will depend on many geological, chemical, and physical factors, as elaborated on in relevant experimental results[37,49,51,70]. While the specific depth at which amphibole-mediated SCSS reduction will occur is variable, the important feature to note about this model is that amphibole represents a bridge between the magnetite-dominated and garnet-dominated petrological models proposed in recent years. As these semi-mature arcs evolve, garnet will fill much the same role as amphibole in controlling Fe and stabilizing sulphide. This allows for a certain degree of temporal evolution in the primary petrological vector controlling bulk [Cu] in arc magmas, where one would expect a young, thermally immature arc to modulate its Cu via magnetite[19], evolving to amphibole at a moderate maturity and thickness, culminating in garnet-dominated Cu control by the time the arc

reaches maturity[7].

One point of departure with the analysis in this study as compared to previous studies relates the importance and timing of sulphide saturation. Some studies[7,18] have assumed that early sulphide saturation is detrimental to eventual porphyry copper deposit development, articulating the 'Cu paradox,' of low magmatic [Cu] being associated with ore deposits[7]. Studies using platinum group elements as proxies for sulphide saturation in arc systems make this assumption more explicit, arguing that ore development requires late sulphide saturation[18]. However, as suggested in recent work[24], porphyry systems that have experienced both prolonged amphibole fractionation and early sulphide crystallization (and subsequent Cu loss) seem perfectly capable of developing porphyry deposits later in their lifetime[24]. The global analysis shown here appears to confirm that melt Cu concentration does not act as a primary control on the potential of a magma to go on and make a porphyry deposit. Similarly, this amphibole-mediated SCSS reduction model does not imply that amphibole fractionation is a critical missing link leading to porphyry development. Rather, widespread amphibole fractionation (as reflected by the petrography and/or whole-rock chemistry of a magma) is a consequence of particular magmatic conditions (P, T, fO_2) that might, under the right geological conditions, signal the right environment to develop a porphyry. Thus, amphibole is seen as a driver of melt chemistry and SCSS changes, but more an indicator of, rather than a driver of, porphyry development. In agreement with the observation that high Sr/Y magmas have lower Cu concentrations[3,7] (Figure 3c), this analysis finds that combined amphibole and/or garnet fractionation of whole rock chemistry (Figure 4,5) can lead to early sulphide saturation (Figure 7,8). The low magmatic Cu concentrations observed in the high Sr/Y magmas in this database are fundamentally the consequence of the deep, hydrous evolution of

arc magmas magmas. This crustal processing can lead to higher magmatic H_2O, promoting amphibole +/- garnet stabilization, and subsequently lower the SCSS enough to precipitate sulphides and reduce magmatic [Cu]. While this implies that amphibole-dominated fractionation is thus a consequence of, rather than the cause of, magmas being able to form porphyry deposits, amphiboles abundance in deep-crust magmas is readily detectable by whole rock geochemistry, and could be used alongside other proxies to assess magmatic ore potential in porphyry settings.

5 Conclusion

In this study we present a comprehensive geochemical and geophysical database of volcanic whole rock samples across 17 arcs covering most of the Earth's active subduction zones. This database, ArcMetals, is differentiated from previous efforts by a rigorous filtration and data compilation strategy. Here, we present the first order features of thisArcMetals alongside a simple trace element and sulphide saturation model to identify the key petrological processes that control [Cu] in arc magmas. More importantly, there is a strong association between high Sr/Y, calc-alkaline differentiation, and amphibole +/- garnet fractionation in conditions relevant to porphyry deposits. High Sr/Y magmas show depletion of FeO during calc-alkaline differentiation and are associated with significantly lower whole rock mean Cu concentrations and thicker continental crust. We show that trends are driven by extensive amphibole fractionation at temperatures below 1050°C, which lowers melt FeO (and other major elements) and hence SCSS, driving widespread andesitic sulphide saturation and the removal of Cu into early forming sulphide melts. As has been shown in previous work, we contend that garnet fractionation can also contribute to Fe depletion, and subsequently increases the likelihood of sulphide saturation at greater depths

before amphibole fractionates[7,59]. However, this is not necessary on its own to stabilize sulphide. Rather, as our models of S in an empirical arc basalt show, even olivine and clinopyroxene can mediate a substantial drop in SCSS, leading to sulphide fractionation. On the whole, sulphide fractionation should be regarded as a widespread phenomenon early on in the history of arc magmas, where processes like magnetite, amphibole, and garnet fractionation contribute to overall changes in melt SCSS and melt [S].

Amphibole, this study's preferred petrological vector, provides a generic explanation for global Cu systematics in semi-mature arc environments, as many calc-alkaline, oxidized arc magmas with (1) moderate to high water contents, (2) stored in the mid to deep crust at (3) moderate temperatures (800-1050°C) are easily able to stabilize and fractionate amphibole, evidenced by Dy/Dy* and λ metrics and empirical data. Importantly, this analysis indicates that amphibole fractionation is, irrespective of the presence of garnet on the liquidus, capable of lowering SCSS and promoting early sulphide saturation, and is a useful indicator of the kind of geological conditions that might lead to later porphyry development. Furthermore, while magmatic Cu contents are found to be reflective of the crucial petrological processes identified in this and other studies, [Cu] is not found to be a primary driver or proxy for ore fertility on its own. Likewise, amphibole fractionation is a consequence of the kinds of conditions conducive to porphyry development, and amphibole could be used as a petrological and geochemical indicator for potential porphyry-developing magmas. While many arc magmas fractionate amphibole[49] and most (if not all) arc magmas are rich in water and other volatiles, porphyry deposits remain rare. This study demonstrates early sulphide saturation is not necessarily detrimental to later porphyry formation from a typical calc-alkaline arc magmas, and that minerals like amphibole don't make porphyries, but rather are associated with

porphyry-friendly physical and chemical conditions. Even more crucial to this process is the tectonic (e.g. compressional stresses), geodynamic, geological, and temporal conditions of the magma reservoir system itself[4,24,25,93], which along with the geochemical factors analyzed here, strongly influence whether or not a porphyry system will form. It is possible that porphyry mineralization requires long timescales for differentiation and fluid segregation[4,25] under conducive crustal configurations, which could promote further amphibole crystallization in a melt-rich mid-crustal hot zone[4]. Larger magma volumes may be optimal for achieving extreme volatile concentration[94] (e.g. minimum 1000 km^3 for Bingham Canyon and other large porphyry deposits[4,27]), which would also favor porphyry mineralization[4,24–26].

References

1. Arndt, N. T. *et al.* Future global mineral resources. *Geochemical Perspectives* **6,** 1–171 (2017).

2. Singer, D. A., Berger, V. I., Menzie, W. D. & Berger, B. R. Porphyry copper deposit density. *Economic Geology* **100,** 491–514 (2005).

3. Richards, J. P. The oxidation state, and sulfur and Cu contents of arc magmas: implications for metallogeny. *Lithos* **233,** 27–45 (2015).

4. Chiaradia, M. & Caricchi, L. Stochastic modelling of deep magmatic controls on porphyry copper deposit endowment. *Scientific reports* **7,** 1–11 (2017).

5. Blundy, J., Mavrogenes, J., Tattitch, B., Sparks, S. & Gilmer, A. Generation of porphyry copper deposits by gas–brine reaction in volcanic arcs. *Nature Geoscience* **8,** 235–240 (2015).

6. Wilkinson, J. J. Triggers for the formation of porphyry ore deposits in magmatic arcs. *Nature Geoscience* **6,** 917. http://dx.doi.org/10.1038/ngeo1940%20http://10.0.4.14/ngeo1940%20https://www.nature.com/articles/ngeo1940#supplementary-information (Oct. 2013).

7. Lee, C.-T. A. & Tang, M. How to make porphyry copper deposits. *Earth and Planetary Science Letters* **529,** 115868 (2020).

8. Richards, J. Tectono-magmatic precursors for porphyry Cu-(Mo-Au) deposit formation. *Economic Geology* **98,** 1515–1533 (2003).

9. Richards, J. P. Magmatic to hydrothermal metal fluxes in convergent and collided margins. *Ore Geology Reviews* **40,** 1–26 (2011).

10. Hedenquist, J. W. & Lowenstern, J. B. The role of magmas in the formation of hydrothermal ore deposits. *Nature* **370,** 519–527. ISSN: 0028-0836. http://www.nature.com/doifinder/10.1038/370519a0 (Aug. 1994).

11. Kiseeva, E. S. & Wood, B. J. A simple model for chalcophile element partitioning between sulphide and silicate liquids with geochemical applications. *Earth and Planetary Science Letters.* ISSN: 0012821X (2013).

12. Kiseeva, E. S., Fonseca, R. O. & Smythe, D. J. Chalcophile elements and sulfides in the upper mantle. *Elements* **13,** 111–116 (2017).

13. Patten, C., Barnes, S.-J., Mathez, E. A. & Jenner, F. E. Partition coefficients of chalcophile elements between sulfide and silicate melts and the early crystallization history of sulfide liquid: LA-ICP-MS analysis of MORB sulfide droplets. *Chemical Geology* **358,** 170–188 (2013).

14. Jugo, P., Candela, P. & Piccoli, P. Magmatic sulfides and Au: Cu ratios in porphyry deposits: an experimental study of copper and gold partitioning at 850 C, 100 MPa in a haplogranitic melt–pyrrhotite–intermediate

solid solution–gold metal assemblage, at gas saturation. *Lithos* **46,** 573–589 (1999).

15. Simon, A. C., Pettke, T., Candela, P. A., Piccoli, P. M. & Heinrich, C. A. Copper partitioning in a melt–vapor–brine–magnetite–pyrrhotite assemblage. *Geochimica et Cosmochimica Acta* **70,** 5583–5600 (2006).

16. Li, Y. & Audétat, A. Effects of temperature, silicate melt composition, and oxygen fugacity on the partitioning of V, Mn, Co, Ni, Cu, Zn, As, Mo, Ag, Sn, Sb, W, Au, Pb, and Bi between sulfide phases and silicate melt. *Geochimica et Cosmochimica Acta.* ISSN: 00167037 (2015).

17. Li, Y. & Audétat, A. Gold solubility and partitioning between sulfide liquid, monosulfide solid solution and hydrous mantle melts: Implications for the formation of Au-rich magmas and crust–mantle differentiation. *Geochimica et Cosmochimica Acta* **118,** 247–262 (2013).

18. Park, J.-W. *et al.* Chalcophile element fertility and the formation of porphyry Cu±Au deposits. *Mineralium Deposita* **54,** 657–670 (2019).

19. Jenner, F. E., ONeill, H. S. C., Arculus, R. J. & Mavrogenes, J. A. The magnetite crisis in the evolution of arc-related magmas and the initial concentration of Au, Ag and Cu. *Journal of Petrology.* ISSN: 00223530 (2010).

20. Chiaradia, M. Copper enrichment in arc magmas controlled by overriding plate thickness. *Nature Geoscience* **7,** 43–46 (2014).

21. Edmonds, M. & Mather, T. A. Volcanic sulfides and outgassing. *Elements.* ISSN: 18115217 (2017).

22. Nadeau, O., Williams-Jones, A. E. & Stix, J. Sulphide magma as a source of metals in arc-related magmatic hydrothermal ore fluids. *Nature Geoscience.* ISSN: 17520894 (2010).

23. Audetat, A., Pettke, T., Heinrich, C. A. & Bodnar, R. J. Special paper: the composition of magmatic-hydrothermal fluids in barren and mineralized intrusions. *Economic Geology* **103,** 877–908 (2008).

24. Du, J. & Audétat, A. Early sulfide saturation is not detrimental to porphyry Cu-Au formation. *Geology* **48,** 519–524 (2020).

25. Loucks, R. Distinctive composition of copper-ore-forming arcmagmas. *Australian Journal of Earth Sciences* **61,** 5–16 (2014).

26. Rezeau, H. & Jagoutz, O. The importance of H2O in arc magmas for the formation of porphyry Cu deposits. *Ore Geology Reviews,* 103744 (2020).

27. Chelle-Michou, C., Rottier, B., Caricchi, L. & Simpson, G. Tempo of magma degassing and the genesis of porphyry copper deposits. *Scientific reports* **7,** 40566 (2017).

28. Steinberger, I., Hinks, D., Driesner, T. & Heinrich, C. A. Source plutons driving porphyry copper ore formation: combining geomagnetic data, thermal constraints, and chemical mass balance to quantify the magma chamber beneath the Bingham Canyon deposit. *Economic Geology* **108,** 605–624 (2013).

29. O'Neill, H. The thermodynamic controls on sulfide saturation in silicate melts with application to Ocean Floor Basalts. (2020).

30. Smythe, D. J., Wood, B. J. & Kiseeva, E. S. The S content of silicate melts at sulfide saturation: new experiments and a model incorporating the effects of sulfide composition. *American Mineralogist* **102,** 795–803 (2017).

31. Jugo, P. J., Wilke, M. & Botcharnikov, R. E. Sulfur K-edge XANES analysis of natural and synthetic basaltic glasses: Implications for S speciation

and S content as function of oxygen fugacity. *Geochimica et Cosmochimica Acta* **74,** 5926–5938 (2010).

32. Kiseeva, E. S. & Wood, B. J. The effects of composition and temperature on chalcophile and lithophile element partitioning into magmatic sulphides. *Earth and Planetary Science Letters* **424,** 280–294 (2015).

33. Zajacz, Z. & Tsay, A. An accurate model to predict sulfur concentration at anhydrite saturation in silicate melts. *Geochimica et Cosmochimica Acta* **261,** 288–304 (2019).

34. Nash, W. M., Smythe, D. J. & Wood, B. J. Compositional and temperature effects on sulfur speciation and solubility in silicate melts. *Earth and Planetary Science Letters* **507,** 187–198. ISSN: 0012-821X. http://www.sciencedirect.com/science/article/pii/S0012821X18307155 (2019).

35. Chiaradia, M. Crustal thickness control on Sr/Y signatures of recent arc magmas: an Earth scale perspective. *Scientific reports* **5,** 8115 (2015).

36. Farner, M. J. & Lee, C.-T. A. Effects of crustal thickness on magmatic differentiation in subduction zone volcanism: a global study. *Earth and Planetary Science Letters* **470,** 96–107 (2017).

37. Ulmer, P., Kaegi, R. & Müntener, O. Experimentally derived intermediate to silica-rich arc magmas by fractional and equilibrium crystallization at 1· 0 GPa: An evaluation of phase relationships, compositions, liquid lines of descent and oxygen fugacity. *Journal of Petrology* **59,** 11–58 (2018).

38. Sarbas, B. & Nohl, U. The GEOROC database as part of a growing geoinformatics network. *Geoinformatics* (2008).

39. Hayes, G. P. *et al.* Slab2, a comprehensive subduction zone geometry model. *Science* **362,** 58–61 (2018).

40. Szwillus, W., Afonso, J. C., Ebbing, J. & Mooney, W. D. Global crustal thickness and velocity structure from geostatistical analysis of seismic data. *Journal of Geophysical Research: Solid Earth* **124,** 1626–1652 (2019).

41. Pasyanos, M. E., Masters, T. G., Laske, G. & Ma, Z. LITHO1. 0: An updated crust and lithospheric model of the Earth. *Journal of Geophysical Research: Solid Earth* **119,** 2153–2173 (2014).

42. Syracuse, E. M. & Abers, G. A. Global compilation of variations in slab depth beneath arc volcanoes and implications. *Geochemistry, Geophysics, Geosystems.* ISSN: 15252027 (2006).

43. Richards, J. P. High Sr/Y ratio magmas and porphyry Cu, Mo, Au Deposits:Just add water. *Economic Geology* **106,** 1075–1081. ISSN: 0361-0128. http://dx.doi.org/10.2113/econgeo.106.7.1075 (Nov. 2011).

44. Ewart, A. & Griffin, W. Application of proton-microprobe data to trace-element partitioning in volcanic rocks. *Chemical Geology* **117,** 251–284 (1994).

45. Green, T. H. Experimental studies of trace-element partitioning applicable to igneous petrogenesis—Sedona 16 years later. *Chemical Geology* **117,** 1–36 (1994).

46. Grove, T., Parman, S., Bowring, S., Price, R. & Baker, M. The role of an H 2 O-rich fluid component in the generation of primitive basaltic andesites and andesites from the Mt. Shasta region, N California. *Contributions to Mineralogy and Petrology* **142,** 375–396 (2002).

47. Stolper, E. Water in silicate glasses: an infrared spectroscopic study. *Contributions to Mineralogy and Petrology* **81,** 1–17 (1982).

48. Foden, J. & Green, D. Possible role of amphibole in the origin of andesite: some experimental and natural evidence. *Contributions to Mineralogy and Petrology* **109,** 479–493 (1992).

49. Ridolfi, F., Renzulli, A. & Puerini, M. Stability and chemical equilibrium of amphibole in calc-alkaline magmas: an overview, new thermobarometric formulations and application to subduction-related volcanoes. *Contributions to Mineralogy and Petrology* **160,** 45–66 (2010).

50. Santana, L. V., McLeod, C., Blakemore, D., Shaulis, B. & Hill, T. Bolivian hornblendite cumulates: Insights into the depths of Central Andean arc magmatic systems. *Lithos,* 105618 (2020).

51. Alonso-Perez, R., Müntener, O. & Ulmer, P. Igneous garnet and amphibole fractionation in the roots of island arcs: experimental constraints on andesitic liquids. *Contributions to Mineralogy and Petrology* **157,** 541 (2009).

52. Lee, C.-T. A. *et al.* Copper systematics in arc magmas and implications for crust-mantle differentiation. *Science* **336,** 64–68 (2012).

53. Jenner, F. E. Cumulate causes for the low contents of sulfide-loving elements in the continental crust. *Nature Geoscience.* ISSN: 17520908 (2017).

54. Davidson, J., Turner, S. & Plank, T. Dy/Dy*: variations arising from mantle sources and petrogenetic processes. *Journal of Petrology* **54,** 525–537 (2013).

55. Chen, K. *et al.* Sulfide-bearing cumulates in deep continental arcs: The missing copper reservoir. *Earth and Planetary Science Letters,* 115971 (2019).

56. Cox, D., Watt, S. F., Jenner, F. E., Hastie, A. R. & Hammond, S. J. Chalcophile element processing beneath a continental arc stratovolcano. *Earth and Planetary Science Letters* **522,** 1–11 (2019).

57. O'Neill, H. S. C. The smoothness and shapes of chondrite-normalized rare earth element patterns in basalts. *Journal of Petrology* **57,** 1463–1508 (2016).

58. Sullivan, L. *Hypothesis Testing - Analysis of Variance (ANOVA)* https://sphweb.bumc.bu.edu/otlt/MPH-Modules/BS/BS704_HypothesisTesting-ANOVA/BS704_HypothesisTesting-Anova_print.html.

59. Cox, D. *et al.* Elevated magma fluxes deliver high-Cu magmas to the upper crust. *Geology* **48** (2020).

60. Greene, A. R., DeBARI, S. M., Kelemen, P. B., Blusztajn, J. & Clift, P. D. A detailed geochemical study of island arc crust: the Talkeetna arc section, south–central Alaska. *Journal of Petrology* **47,** 1051–1093 (2006).

61. Bissig, T., Leal-Meja, H., Stevens, R. B. & Hart, C. J. High Sr/Y magma petrogenesis and the link to porphyry mineralization as revealed by Garnet-Bearing I-type granodiorite porphyries of the Middle Cauca Au-Cu Belt, Colombia. *Economic Geology* **112,** 551–568 (2017).

62. Petterson, M. The plutonic crust of Kohistan and volcanic crust of Kohistan–Ladakh, north Pakistan/India: lessons learned for deep and shallow arc processes. *Geological Society, London, Special Publications* **483,** 123–164 (2019).

63. Jan, M. Q. & Howie, R. The mineralogy and geochemistry of the metamorphosed basic and ultrabasic rocks of the Jijal complex, Kohistan, NW Pakistan. *Journal of Petrology* **22,** 85–126 (1981).

64. Ducea, M. N., Saleeby, J. B. & Bergantz, G. The architecture, chemistry, and evolution of continental magmatic arcs. *Annual Review of Earth and Planetary Sciences* **43,** 299–331 (2015).

65. Feigenson, M. D. & Carr, M. J. The source of Central American lavas: inferences from geochemical inverse modeling. *Contributions to Mineralogy and Petrology* **113,** 226–235 (1993).

66. Jeffery, A. J. *et al.* The pre-eruptive magma plumbing system of the 2007–2008 dome-forming eruption of Kelut volcano, East Java, Indonesia. *Contributions to Mineralogy and Petrology* **166,** 275–308 (2013).

67. Hürlimann, N. *et al.* Primary magmas in continental arcs and their differentiated products: petrology of a post-plutonic dyke suite in the Tertiary Adamello batholith (Alps). *Journal of Petrology* **57,** 495–534 (2016).

68. Baker, M. B., Grove, T. L. & Price, R. Primitive basalts and andesites from the Mt. Shasta region, N. California: products of varying melt fraction and water content. *Contributions to Mineralogy and Petrology* **118,** 111–129 (1994).

69. Shaw, D. M. *et al. Trace elements in magmas: a theoretical treatment* (Cambridge University Press, 2006).

70. Nandedkar, R. H., Hürlimann, N., Ulmer, P. & Müntener, O. Amphibole–melt trace element partitioning of fractionating calc-alkaline magmas in the lower crust: an experimental study. *Contributions to Mineralogy and Petrology* **171,** 71 (2016).

71. Leake, B. E. *et al.* Nomenclature of amphiboles; report of the subcommittee on amphiboles of the International Mineralogical Association, Commission on New Minerals and Mineral Names. *The Canadian Mineralogist* **35,** 219–246 (1997).

72. O'Neill, H. & Mavrogenes, J. A. The sulfide capacity and the sulfur content at sulfide saturation of silicate melts at 1400 C and 1 bar. *Journal of Petrology* **43,** 1049–1087 (2002).

73. Fortin, M.-A., Riddle, J., Desjardins-Langlais, Y. & Baker, D. R. The effect of water on the sulfur concentration at sulfide saturation (SCSS) in natural melts. *Geochimica et Cosmochimica Acta* **160,** 100–116 (2015).

74. Jugo, P. J. Sulfur content at sulfide saturation in oxidized magmas. *Geology* **37,** 415–418 (2009).

75. Wallace, P. J. & Edmonds, M. The sulfur budget in magmas: evidence from melt inclusions, submarine glasses, and volcanic gas emissions. *Reviews in Mineralogy and Geochemistry* **73,** 215–246 (2011).

76. Frost, B. R. *et al.* A geochemical classification for granitic rocks. *Journal of petrology* **42,** 2033–2048 (2001).

77. Wieser, P., Jenner, F., Edmonds, M., Maclennan, J. & Kunz, B. Chalcophile elements track the fate of sulfur at Kilauea Volcano, Hawai'i (2020).

78. Li, Y. & Audetat, A. Partitioning of V,Mn, Co, Ni,Cu,Zn,As,Mo,Ag,Sn,Sb,W,Au,Pb, and Bi between sulphide phases and hydrous basanite melt at upper mantle conditions. *Earth and Planetary Science Letters* (2012).

79. Collins, S., Maclennan, J., Pyle, D., Barnes, S.-J. & Upton, B. Two phases of sulphide saturation in Réunion magmas: Evidence from cumulates. *Earth and Planetary Science Letters* **337,** 104–113 (2012).

80. Kamenetsky, V. S. *et al.* Silicate-sulfide liquid immiscibility in modern arc basalt (Tolbachik volcano, Kamchatka): Part II. Composition, liquidus assemblage and fractionation of the silicate melt. *Chemical Geology* **471,** 92–110 (2017).

81. Kamenetsky, V. S. & Zelenski, M. Origin of noble-metal nuggets in sulfide-saturated arc magmas: A case study of olivine-hosted sulfide melt inclusions from the Tolbachik volcano (Kamchatka, Russia). *Geology* **48,** 620–624 (2020).

82. Zelenski, M., Kamenetsky, V., Mavrogenes, J., Gurenko, A. & Danyushevsky, L. Silicate-sulfide liquid immiscibility in modern arc basalt (Tolbachik volcano, Kamchatka): Part I. Occurrence and compositions of sulfide melts. *Chemical Geology* **478,** 102–111 (2018).

83. Nadeau, O., Stix, J. & Williams-Jones, A. E. The behavior of Cu, Zn and Pb during magmatic–hydrothermal activity at Merapi volcano, Indonesia. *Chemical Geology* **342,** 167–179 (2013).

84. Berlo, K., van Hinsberg, V., Vigouroux, N., Gagnon, J. & Williams-Jones, A. Sulfide breakdown controls metal signature in volcanic gas at Kawah Ijen volcano, Indonesia. *Chemical Geology* **371,** 115–127 (2014).

85. Nadeau, O., Stix, J. & Williams-Jones, A. E. Links between arc volcanoes and porphyry-epithermal ore deposits. *Geology.* ISSN: 19432682 (2016).

86. Georgatou, A., Chiaradia, M., Rezeau, H. & Wälle, M. Magmatic sulphides in Quaternary Ecuadorian arc magmas. *Lithos* **296,** 580–599 (2018).

87. Chang, J. & Audétat, A. Petrogenesis and metal content of hornblende-rich xenoliths from two Laramide-age magma systems in southwestern USA: insights into the metal budget of arc magmas. *Journal of Petrology* **59,** 1869–1898 (2018).

88. Keith, M., Haase, K. M., Klemd, R., Schwarz-Schampera, U. & Franke, H. Systematic variations in magmatic sulphide chemistry from mid-ocean ridges, back-arc basins and island arcs. *Chemical Geology.* ISSN: 00092541 (2017).

89. Rottier, B., Audétat, A., Koděra, P. & Lexa, J. Origin and Evolution of Magmas in the Porphyry Au-mineralized Javorie Volcano (Central Slovakia): Evidence from Thermobarometry, Melt Inclusions and Sulfide Inclusions. *Journal of Petrology* **60,** 2449–2482 (2019).

90. Jenner, F. E. *et al.* Chalcophile element systematics in volcanic glasses from the northwestern Lau Basin. *Geochemistry, Geophysics, Geosystems.* ISSN: 15252027 (2012).

91. Holland, H. D. & Turekian, K. K. Treatise on geochemistry (2004).

92. Jenner, F. E. & Arevalo, R. D. Major and trace elerment analysis of natural and experimental igneous systems using LA-ICP-MS. *Elements.* ISSN: 18115217 (2016).

93. Richards, J. P. A Shake-Up in the Porphyry World? *Economic Geology* **113,** 1225–1233. ISSN: 0361-0128. http://dx.doi.org/10.5382/econgeo.2018.4589 (Sept. 2018).

94. Rohrlach, B. D., Loucks, R. R. & Porter, T. Multi-million-year cyclic ramp-up of volatiles in a lower crustal magma reservoir trapped below the Tampakan copper-gold deposit by Mio-Pliocene crustal compression in the southern Philippines. *Super porphyry copper and gold deposits: A global perspective* **2,** 369–407 (2005).

Data Availability

All of our data, code, and protocols are available at the corresponding author's GitHub: https://github.com/ndb38/slab_metals. This current link is subject to change: the database and all associated code is going to be stream lined into a less crowded repository in future versions, and allowed to virtually run through Binder. The code and figures will be updated in future versions of the database, but all the material pertaining to this paper will be preserved.

Acknowledgements

We thank Callum Reekie for providing the Python code for the SCSS models, and for useful comments on SCSS. We thank Penny Wieser for providing a critical appraisal of our early database, and helpful comments regarding the SCSS and trace elements models and their outputs. An additional thank you is extended to James Crosby and Andrew Whyte for their early comments on the importance of amphibole. We would also like to thank Cin-Ty Lee, Massimo Chiaradia, Adam Simon, and two anonymous reviewers for their constructive comments on an earlier version of this manuscript. We would also like to thank the attendees of Goldschmidt 2020 for their constructive and supportive comments. We acknowledge funding from the NERC Centre for the Observation and Modelling of Earthquakes, Volcanoes and Tectonics (COMET). The Gates Cambridge Trust provides financial support for NDB's PhD.

Author Contributions

NDB conceived the project with advice and comments from ME and FJ. NDB compiled the database, wrote the Python code, and performed the analysis. ME., FJ, AA, and HW provided equal contributions regarding data interpretations and significant references. NDB wrote the manuscript with equal editing contributions from ME, FJ, AA, and HW.

Competing Interests

The authors declare no competing interests.

Materials and Correspondence

All correspondence should be directed to Nicholas Barber (ndb38@cam.ac.uk).

Figures

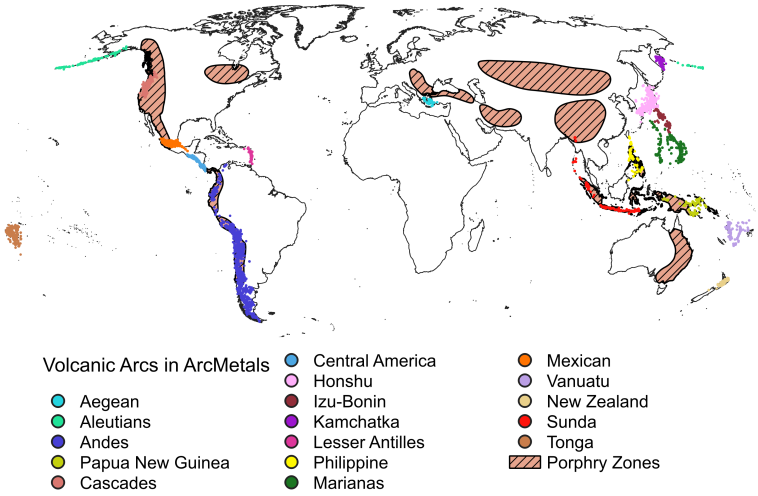

Figure 1: Global distribution of samples used in ArcMelts2, our global data compilation. Sample locations are color coded by arc. Samples are overlayed on zones of porphyry mineralization, taken from [2]. Created using QGIS 3.10.

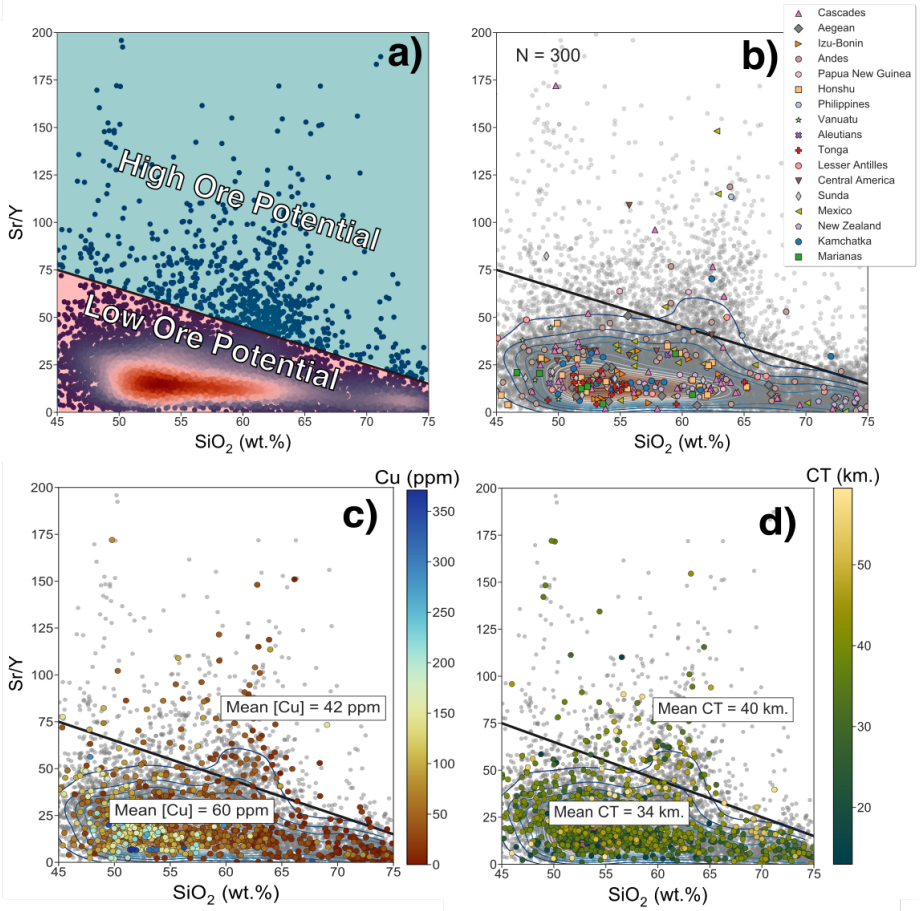

Figure 2: Sr/Y vs. SiO_2 plots, colored for different features. Plots b) and c) are both sub-sampled to only display 300 (b) and 1000 (c) samples for visual clarity. The black line called out in a) differentiates "high" from "low" ore potential, as defined in the literature [25]. Magmas sitting above the black line have higher ore formation potential. Plot a) is colored by the density of points in the total dataset, and contours for sample density are included in all subsequent plots. Plot b) shows a sub-sample of arc magmas colored and symbolized by arc; notice how ore-producing arcs are the only ones that tend to proliferate above the high ore potential line. Plot c) shows a sub-sample of the database colored for Cu, where high and low ore potential magmas have mean [Cu] of 42 and 60 respectively. Similarly, plot d) shows that high ore potential magmas have thicker crust, on average, than low ore potential magmas

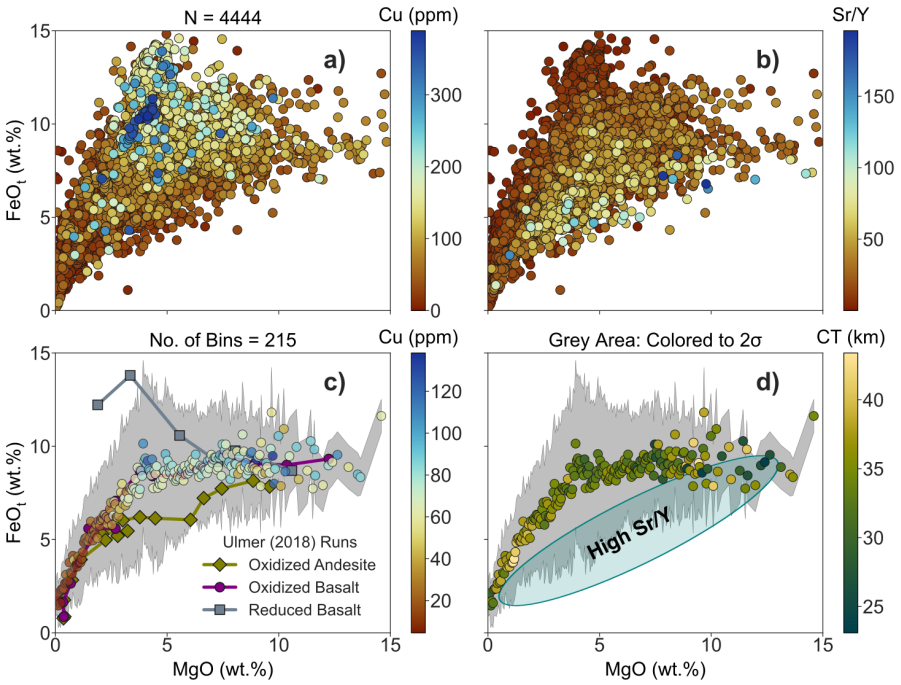

Figure 3: Differentiation trends for the entire dataset, colored for Cu in a) and Sr/Y in b). The highest Cu and Sr/Y measurements are ordered to plot on top of lower measurements. In (c) and (d), resampled averages are calculated for the full database (N = < 12,000) every 0.05 wt.% of MgO, colored for c) Cu (ppm) and d) Crust Thickness (km.). Errors colored out to 2σ, smoothed by a factor of 1.5 to reduce observed spread. Superimposed on the global database (c) are the empirical results of fractional crystallization experiments in arc conditions from [37]. Like Figure 5, blue ellipse is the area where high Sr/Y magmas plot in this Figure (5d)

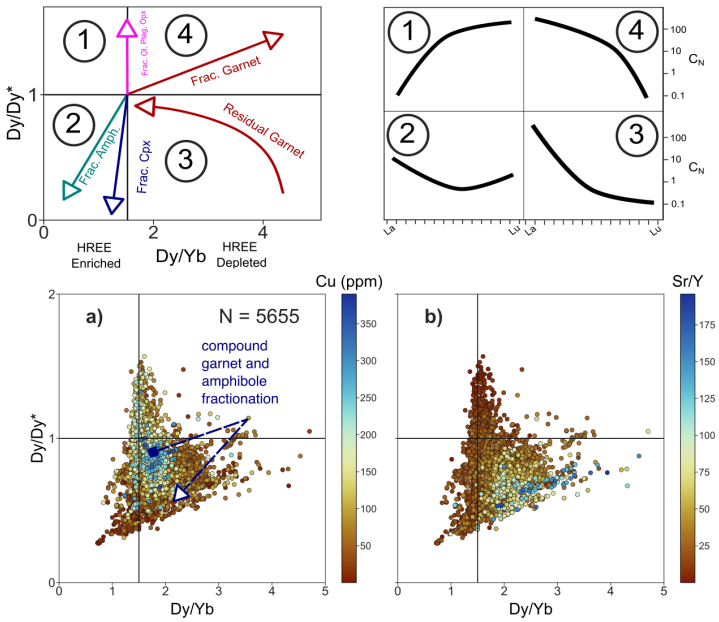

Figure 4: Panels showing the distribution of a) Cu and b) Sr/Y in Dy/Dy vs. Dy/Yb space. These Dy plots show relative fractionation trends according to which mineral phase is dominant. The starting point of each schematic mineral vector is in reference to a chrondrite normalized REE composition. The lowest Cu and highest Sr/Y magmas sit in an area generated by a combination of amphibole and garnet fractionation, and potential mantle source garnet melting. Points in a) and b) are ordered highest to lowest, with the highest Cu and Sr/Y stacked on top. Also shown as a blue ellipse is the area where high Sr/Y magmas plot in Dy/Dy* vs. Dy/Yb space. The dark blue arrow in plot a) shows the expected differentiation path of a magma ascending from high to low pressure, and experiencing first garnet, then amphibole fractionation. Such a liquid line of descent (LLD) can explain the spread in our high ore potential field.

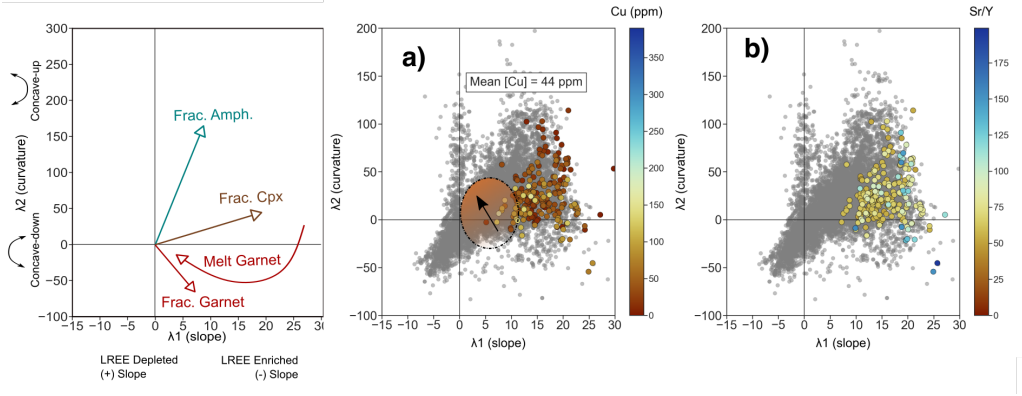

Figure 5: REE behaviour as described by λ spider-plot shape parameters [57]. Top panels are schematics, showing how $\lambda 1$ vs. $\lambda 2$ plots describe mineralogical controls on REEs during differentiation. While $\lambda 1$ describes slope, it is calculated according to the radius of ordered REEs. Hence, a negative $\lambda 1$ corresponds to a positively sloped REE spider profile. a) and b) plot $\lambda 1$ vs. $\lambda 2$ colored for Cu and Sr/Y respectively. Grey points show the entire global database. Colored points are those that plot in the high ore potential field of Figure 3. Mean [Cu] of high Sr/Y field given in a). Empirical results from [37] are shown in the orange shaded area in Figures a) and b), where the arrow denotes the evolving REE contents of empirical products in λ space.

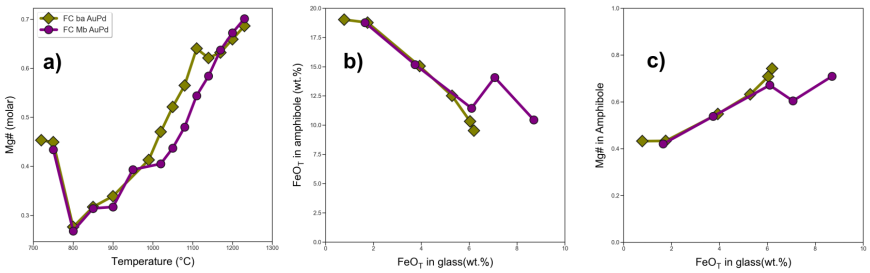

Figure 6: Compilation of melt compositions as compared to the crystallization time and chemistry of amphibole in the empirical products analyzed in this study[37]. Plot a) shows the melt Mg# as a function of temperature - amphibole stabilizes at 1050°C for both FC ba AuPd and FC Mb AuPd. Plot b) shows the FeO content of amphibole plotted against the FeO content of the corresponding silicate melt. Panel c) shows the amphiboles Mg# plotted against silicate melt FeO.

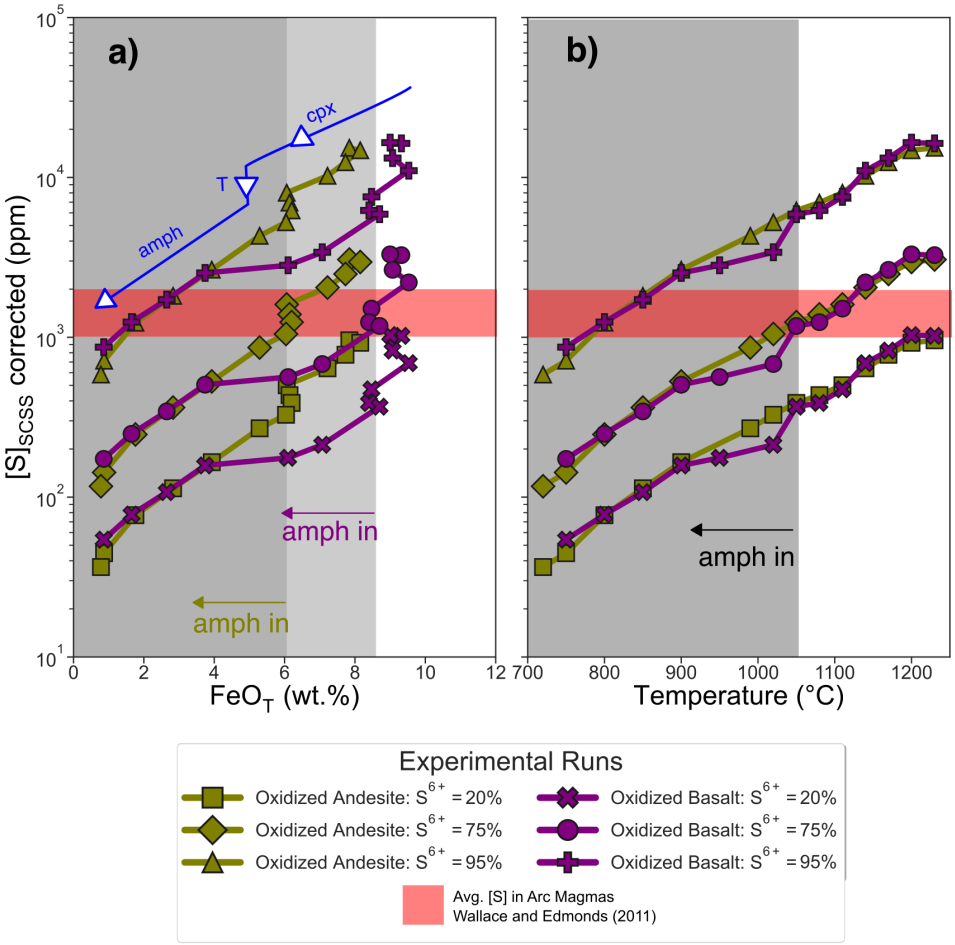

Figure 7: Empirical results of glasses from [37], using initial trace element abundances from [46, 67, 68], and the SCSS model of [29]. Plots show log(SCSS) vs. a) Total FeO and b) c) log(SCSS) vs. Temperature °C. Starting materials in each run were symbolized as: olive colored diamonds = oxidized andesite; purple circles = oxidized basalt;. Vertical grey bars indicate the onset of amphibole fractionation for the oxidized andesite vs. the oxidized basalt runs, respectively. Amphibole is measured to appear around 6.5 wt.% FeO and 1050 °C). SCSS of the model andesite was reported for 3 proportions of $S^{6+}/\Sigma S$ - 20%, 50%, and 90% respectively, following the corrections in [77]. The red box covering the area between 1000 and 2000 ppm [S] is the average minimum [S] content in arc magmas, taken from [75]. The thick blue line and associated blue labels show the inferred dominant-control on SCSS at different steps in the model. Discussion of partition coefficients used to model SCSS, Cu, and Sr/Y can be found in the main text and and Supporting Information)

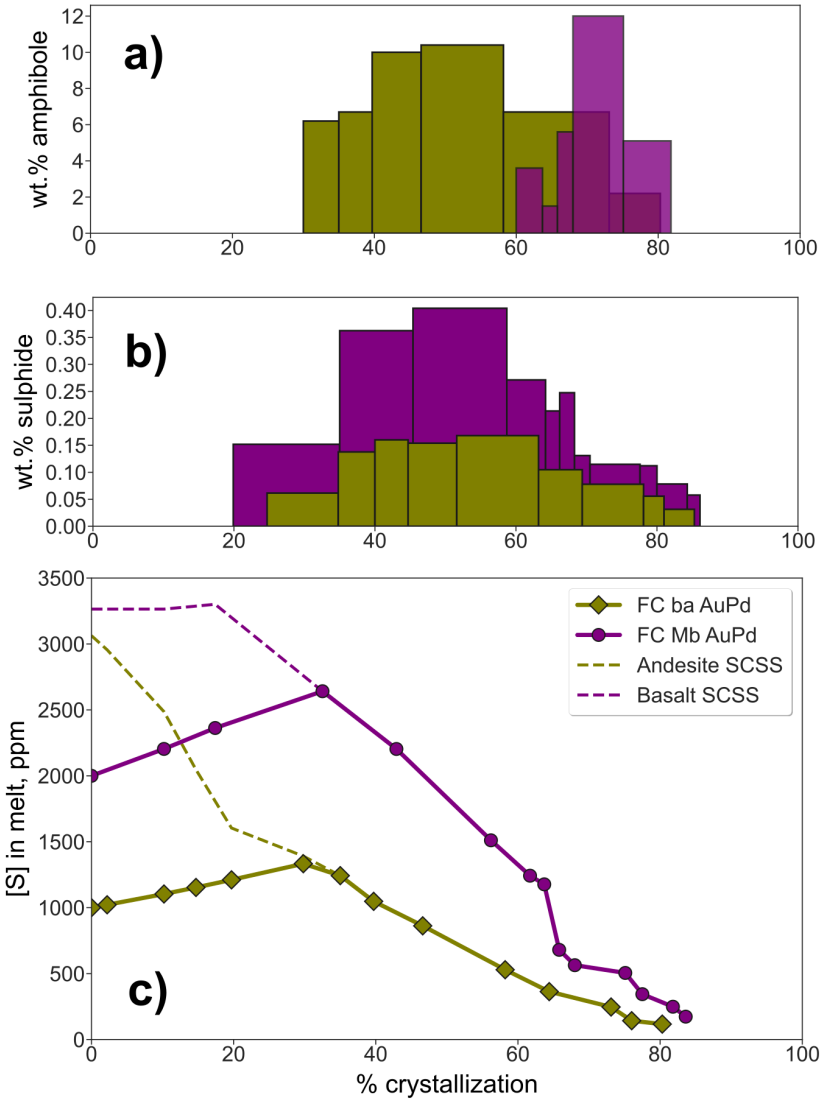

Figure 8: Mass balance of sulphur and sulphide in empirical datasets of oxidized calc-alkaline andesite (FC ba AuPd) and basalt (FC Mb AuPd)[37]. Panel a) shows the mass fractionation of amphibole crystallizing at each step in the experiments of Ulmer et al. 2018. The mass balance model for sulphur and sulphide, discussed in the text (Section 4.3.4) provides estimates of b) the mass of sulphide melt precipitating at each experimental step, and c) the trend in [S] in these kinds of melts. Initial [S] values were fixed at 2000 ppm for the basalt, and 1000 ppm for the andesite (see text for details). The precipitating sulphide had its composition adapted from average sulphide melts at Merapi volcano, Indonesia[22]

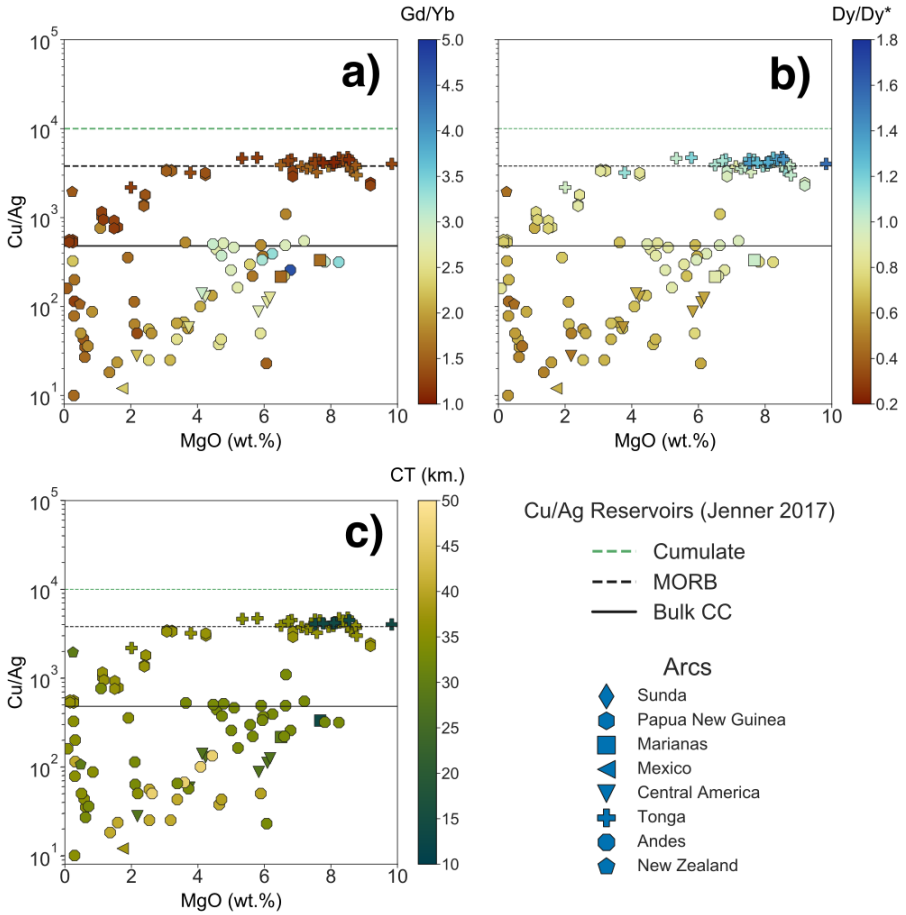

Figure 9: Cu/Ag (as a proxy for crystalline sulphide fractionation) plotted against MgO. Colored for a) Gd/Yb, b) Dy/Dy*, and c) Crust Thickness. Majority of samples plotted here are whole rock compositions. Individual samples are symbolized according to the arc they come from. Plot structure and reference lines for Cu/Ag adapted from [53], as are the reference compositions for Cu/Ag in Sulphide cumulates, MORB, and Bulk CC.

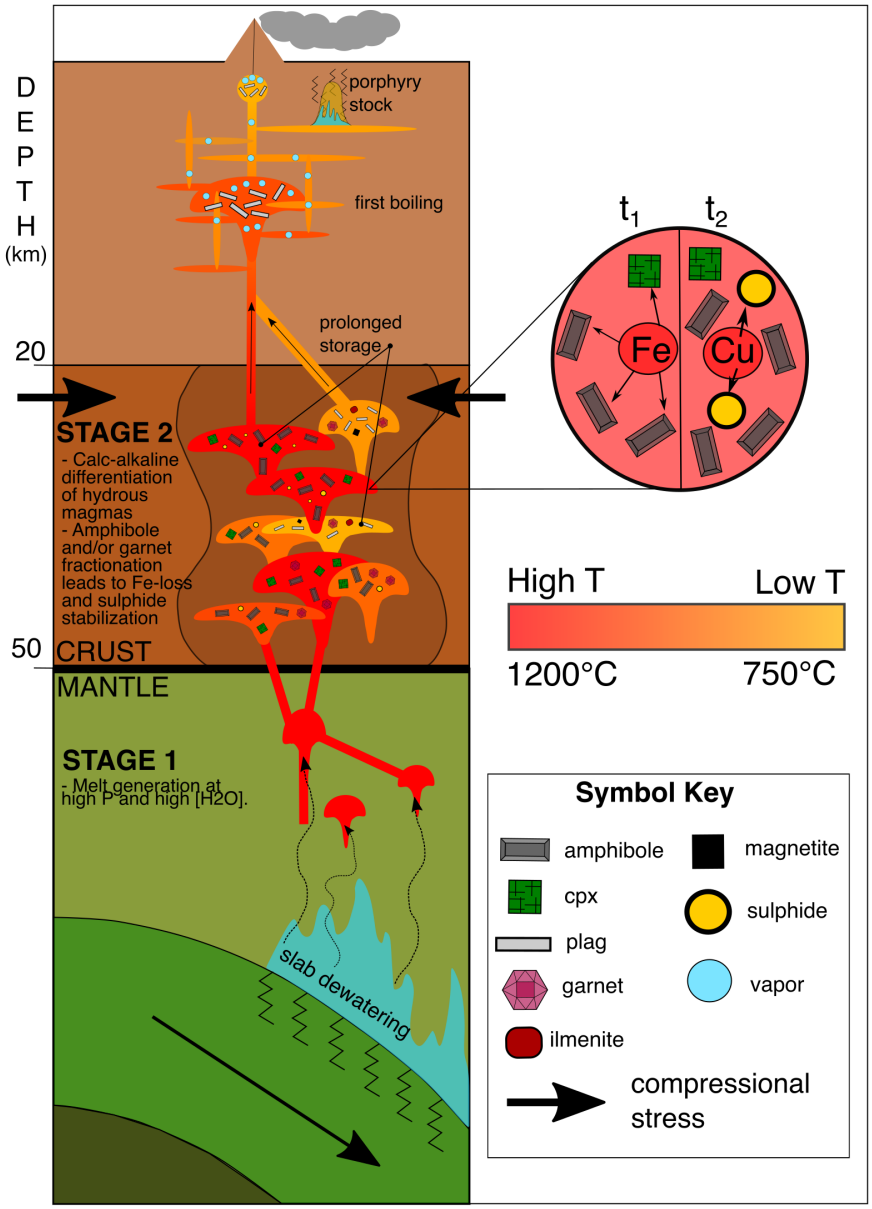

Figure 10: Our proposed model for Cu depletion in arc magmas. This model takes into account the different geochemical and geophysical signals picked out by our database. Stage 1 sees hydrous melting stabilize garnet in the mantle wedge under the right conditions, which imparts the Gd/Yb signal seen in some magmas in Figure 7. High water contents of these calc-alkaline primitive melts contribute to prolonged amphibole fractionation in Stage 2, where magmas staled at depth (=/< 1 GPa) will fractionate enough amphibole to reduce [Fe] and stabilize sulphide. garnet fractionation likely plays a role at depths > 50 km, and could similarly deplete ore-fertile magmas in Fe, leading to sulphide fractionation.